Accepted Manuscript

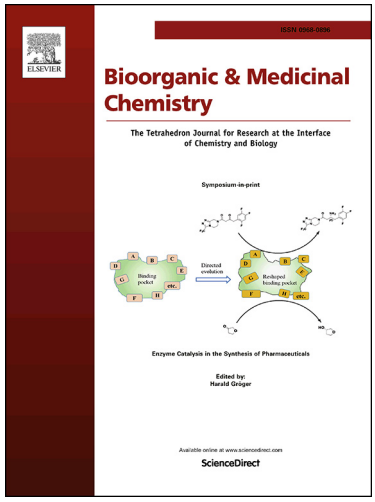

Discovery of DC_H31 as Potential mutant IDH1 Inhibitor through NADPH-based High Throughput Screening

Zhe Duan, Jingqiu Liu, Liping Niu, Jun Wang, Mingqian Feng, Hua Chen, Cheng Luo

PII: S0968-0896(19)30606-6
DOI: https://doi.org/10.1016/j.bmc.2019.05.040
Reference: BMC 14927

To appear in: *Bioorganic & Medicinal Chemistry*

Received Date: 12 April 2019
Revised Date: 24 May 2019
Accepted Date: 27 May 2019

Please cite this article as: Duan, Z., Liu, J., Niu, L., Wang, J., Feng, M., Chen, H., Luo, C., Discovery of DC_H31 as Potential mutant IDH1 Inhibitor through NADPH-based High Throughput Screening, *Bioorganic & Medicinal Chemistry* (2019), doi: https://doi.org/10.1016/j.bmc.2019.05.040

Discovery of DC_H31 as Potential mutant IDH1 Inhibitor through NADPH-based High Throughput Screening

Zhe Duan[a], Jingqiu Liu[b], Liping Niu[c], Jun Wang [b], Mingqian Feng[a*], Hua Chen [c*], Cheng Luo[b*]

a College of Life Science and Technology, Huazhong Agricultural University, Wuhan 430070, China

b State Key Laboratory of Drug Research, Shanghai Institute of Materia Medica, Chinese Academy of Sciences, Shanghai 201203 P. R. China

c Key Laboratory of Chemical Biology of Hebei Province, College of Chemistry and Environmental Science, Hebei University, Bao ding 071002, China

These authors contributed equally: Zhe Duan and Jingqiu Liu

*Corresponding authors

fengmingqian@mail.hzau.edu.cn

Cheng Luo: cluo@simm.ac.cn

Hua Chen: hua-todd@163.com

Abstract:

IDH1 mutations are early events in the development of IDH-mutant gliomas and leukemias and are associated with various regulation of molecular process. Mutations of active site in IDH1 could lead to high levels of 2-HG and the suppression of cellular differentiation, while these changes can be reversed by molecule inhibitors target mutant IDH1. Here, through in-house developed enzymatic assay-based high throughput screening platform, we discovered DC_H31 as a novel IDH1-R132H/C inhibitor, with the IC_{50} value of 0.41 μmol/L and 2.7 μmol/L respectively. In addition, saturable SPR binding assay indicated that DC_H31 bound to IDH1-R132H/C due to specific interaction. Further computational docking studies and structure-activity relationship (SAR) suggest that DC_H31 could occupy the allosteric pocket between the two monomers of IDH1-R132H homodimer, which accounts for its inhibitory ability. And it is possible to conclude

that DC_H31 acts via an allosteric mechanism of inhibition. At the cellular level, DC_H31 could inhibit cell proliferation, promote cell differentiation and reduce the production of 2-HG with a dose-dependent manner in HT1080 cells. Taken together, DC_H31 is a potent selective inhibitor of IDH1-R132H/C both in vitro and in vivo, which can promote the development of more potent pan-inhibitors against IDH1-R132H/C through further structural decoration and provide a new insight for the pharmacological treatment of gliomas.

Keywords: IDH1 mutation; high-throughput Screening; pan-inhibitor; 2-HG; gliomas

Graphical abstract:

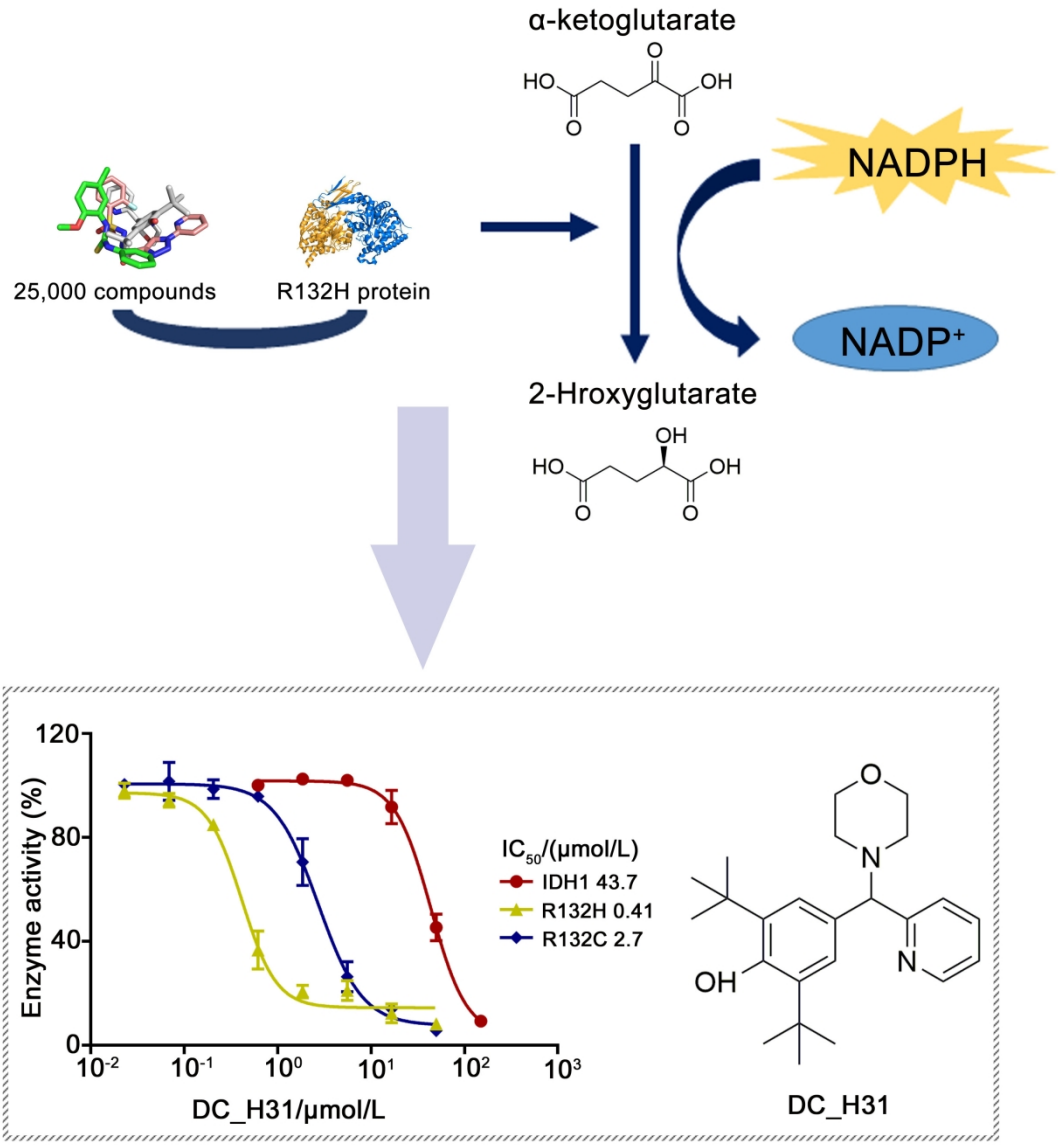

Isocitrate dehydrogenase 1 (IDH1) is a homodimeric metabolic enzyme that participates in lipid metabolism and glycolytic pathway and catalyzes the oxidative decarboxylation of isocitrate to

generate a-ketoglutarate (α-KG) and CO2, accompanied with consuming NADP+ to produce NADPH[1]. Whole-genome sequencing revealed IDH1 mutations were frequent in low-grade gliomas (70-80%) and acute myeloid leukemia (AML) (10-15%)[2-4]. The most prevalent heterozygous mutated residues in IDH1 are located in the enzyme active cavity corresponding to amino acid residue 132[5] that replaces an active-site arginine residue with inactive missense mutation histidine and cystein, accounting to 92%. These mutations render IDH1-R132H/C a neomorphic activity that reduce α-ketoglutarate (α-KG) to the oncometabolite 2-hydroxyglutarate (2-HG) with concomitant reduction of NADPH[6], and finally cause reduction of cellular concentration of α-KG and the accumulation of the D-2HG[7]. α-KG is a substrate of prolyl hydroxylase domain proteins (PHD) which could lead to hydroxylation and degradation of hypoxia inducible factor (HIF). The high level 2-HG may inhibit ten-eleven translocation 2 (TET2), PHD and histone demethylases, which could induce changes in the cell methylome and epigenetic profiles, resulting in blockade of cell differentiation and cell proliferation[8, 9]. Previous studies also demonstrated that the accumulation of 2-HG might be utilized diagnostically in oncology clinics [5, 10-15]. Therefore, due to the pivotal role of IDH1 mutations in tumorigenesis makes IDH1-R132H/C becoming a promising novel therapeutic target . [16].

IDH1 mutations are therapeutically advantageous for inhibiting IDH1-mutant gliomas[17, 18]. There are several types of drugs targeting IDH1 mutations, such as metabolism inhibitors, demethylating agents, and vaccines [5, 19-23]. Small molecule inhibitors targeting mutant IDH1 would lead to reduction of 2-HG and regulate related metabolic pathways. Among the small molecule inhibitors, Ivossidenib (AG-120) is a specific and progressing IDH1-R132H/C inhibitor that restores normal cellular process to AML patients and approved by FDA in 2018 [24, 25]. Nevertheless, there is still urgent need to develop novel pan-inhibitors for IDH1-R132H/C for treatment of gliomas.

In the current study, a new mutation–specific inhibitor, named DC_H31, was identified by a high-throughput screening. DC_H31 can reduce the production of 2-HG in HT1080 cells. The identification of this lead molecule may help us deep understand the mechanism of the action and develop better drugs of the class with improved therapeutic effects.

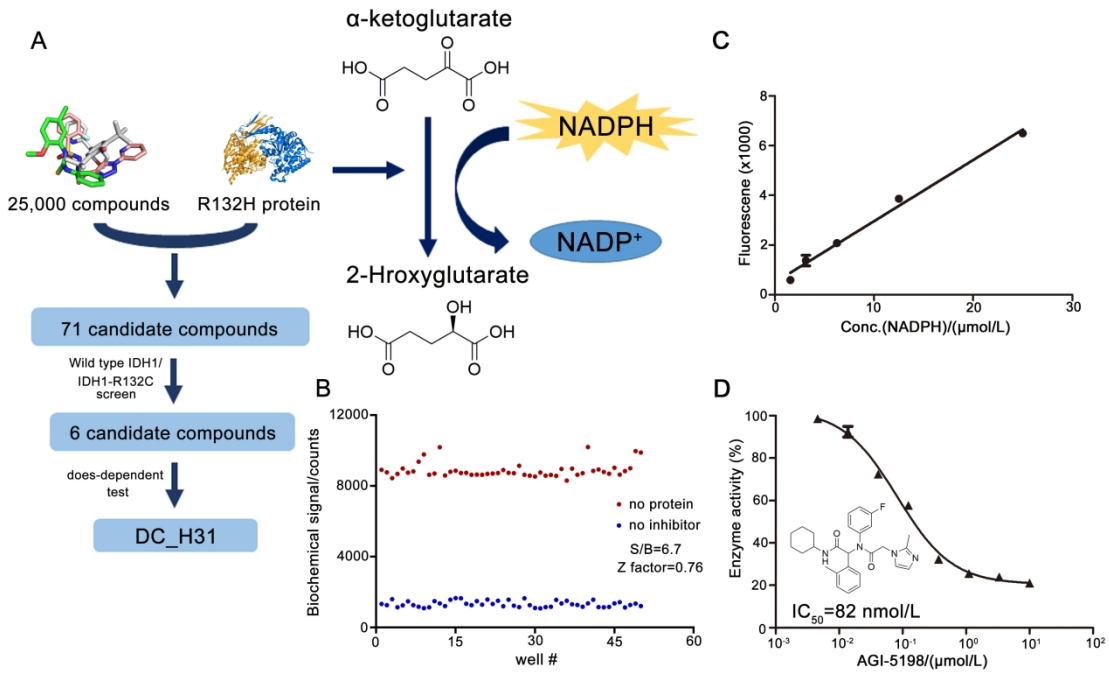

Figure1. The diagram of NADPH-based high throughput screening assay. A) The flowchart of biochemical assay-based high throughput screening for the discovery of DC_H31. **B)** The Z' factor determination of established biochemical assays. **C)** Proportional fluorescence signal at different NADPH concentrations. **D)** The IC_{50} determination of AGI-5198 against IDH1-R132H measured by biochemical assays. (Each point represents the mean ±SD of three replicates)

In our study, a new reliable and robust NADPH-based HTS assay targeting IDH1-R132H/C was developed to identify mutant-specific inhibitor. IDH1-R132H/C catalyze the convert of α-KG to 2-HG mediated with NADPH consumption with a concomitant decrease in fluorescence at 460 nm, therefore inhibition of IDH1-R132H/C enzyme activity by small molecule was evaluated by a fluorescent assays of NADPH depletion. In the assay, the remaining NADPH, which is inversely proportional to IDH1-R132H/C activity, was measured at the endpoint of the reaction by fluorescent reader (λex = 355nm,λem = 460nm) (Fig. 1A), and the fluorescence signal is proportional to the NADPH concentration(Fig. 1C). The Z' factor of the biochemical assay was 0.76 and S/B ratio was 7.6 demonstrated the confidence of this NADPH fluorescence-based biochemical assay(Fig. 1B). The feasibility of this HTS method was further verified by testing the inhibitory activities of the positive compound AGI-5198[17, 18], the IC_{50} value for the compound through this method was 82 nmol/L(Fig. 1D), which was in line with previous reports. All these data demonstrate that the assay is reliable and robust and can be used for molecular screening target mutant IDH1 and wide type (WT) IDH1. Compared to existing mutant IDH1-mediated

NADPH consumption of a diaphorase/resazurin-based detection assay[26], the assay saved diaphorase converts resazurin into resorufin steps, needed less time and simplified screening process for drug discovery of mutant IDH1.

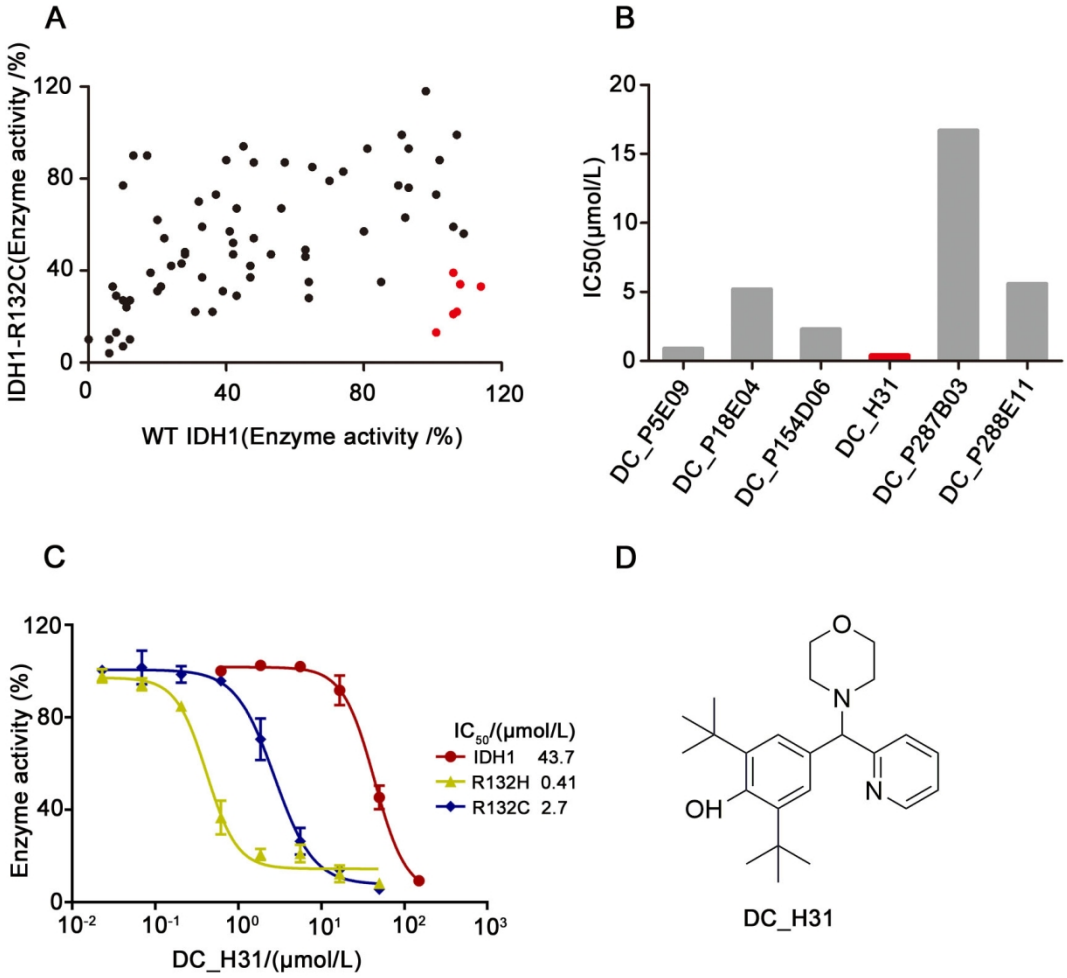

Figure2. The results of high throughput screening and preliminary hit validation. A) Activity of 71 compounds screened from primary HTS in biochemical assays in WT IDH1 (x axis) versus that in IDH1-R132C (y axis). The selected 6 compounds are shown in red. **B)** IC_{50} value of 6 compounds screened from secondary round screening. **C)** The IC_{50} determination of DC_H31 against WT IDH1, IDH1-R132H and IDH1-R132C measured by biochemical assays. (Each point represents the mean ±SD of three replicates. **D)** The chemical structure of DC_H31.

A library containing 25,000 compounds with diverse structures was screened by this NADPH-based HTS assay using DMSO as a negative control and non-enzymatic reaction as a positive control to indicate an inhibition. Through primary HTS with a single concentration (10 μmol/L), 71 compounds which inhibitory activity more than 80% were selected and confirmed in an IDH1-R132C and WT IDH1 assay, and we obtained 6 compounds screened from secondary

round screening, as shown in Figure 2A. After that, all of these 6 compounds were identified by a selection criteria that inhibition as varies with a serious of concentrations between 50 μmol/L to 0.068 μmol/L (Fig. 2B). Finally, DC_H31 was identified as a potential inhibitor with an IC_{50} value of 0.41 μmol/L for IDH1-R132H and 2.7 μmol/L for IDH1-R132C, but inhibited WT IDH1 minimally (Fig. 2C and Fig.2D).

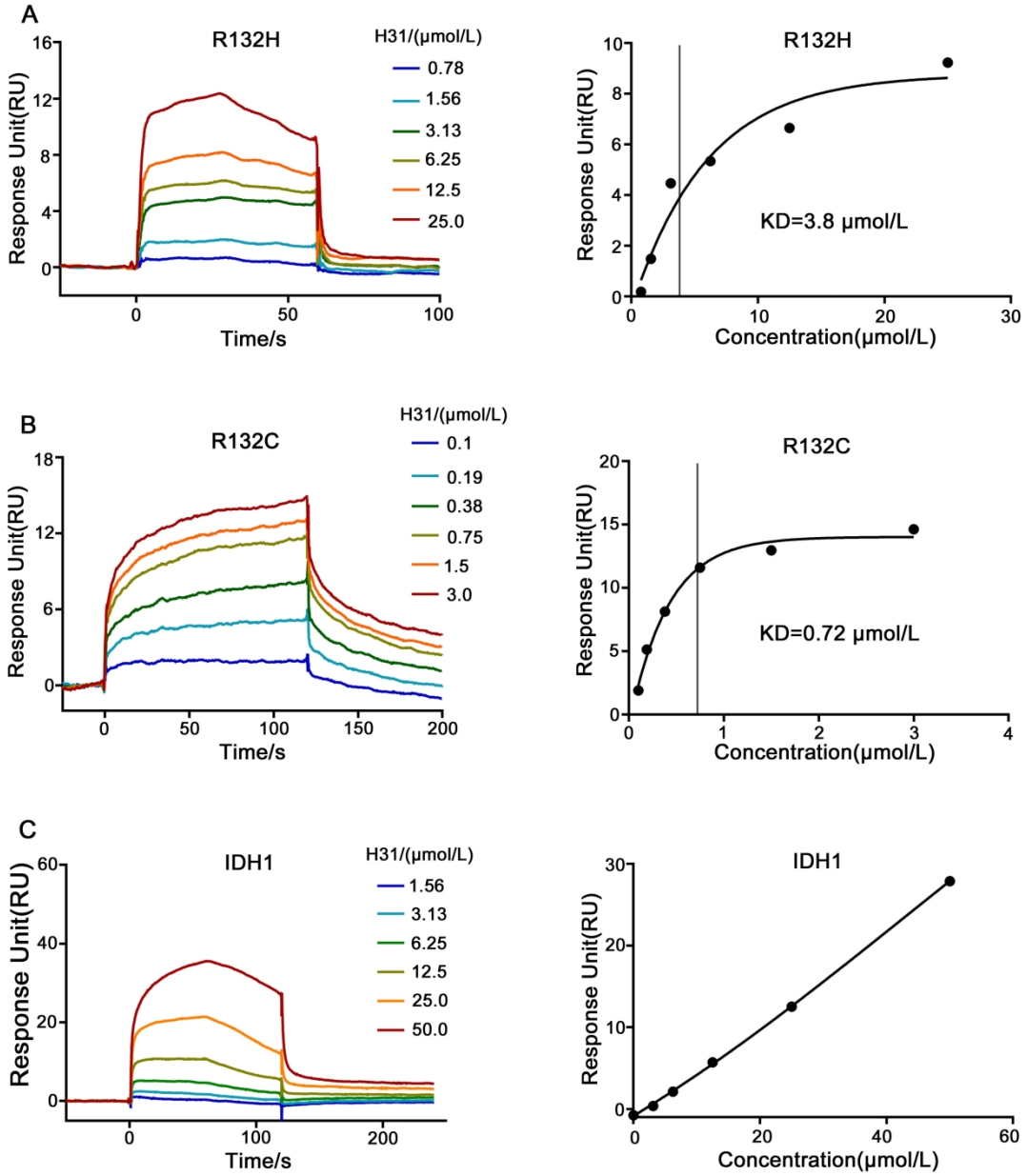

Figure3. DC_H31 binds to IDH1-R132H/C but not WT IDH1 by Surface Plasmon Resonance measurements. **A)** DC_H31 binds to IDH1-R132H with the KD is 3.8 μmol/L. **B)** DC_H31 binds to IDH1-R132C with the KD is 0.72 μmol/L. **C)** DC_H31 could not observably bind to WT IDH1 under the same detection conditions with IDH1-R132H/C.

To further investigating the interaction of compound DC_H31 and IDH1-R132H/C, Surface

Plasmon Resonance (SPR), an optical technique for hit validation [27], was utilized to measure the interactions between the newly discovered DC_H31 towards IDH1-R132H/C and WT IDH1.The data were fit in both kinetic and equilibrium modes. Compound DC_H31 could directly bind to IDH1-R132H and IDH1-R132C with an equilibrium dissociation constant KD of 3.8 μmol/L and 0.72 μmol/L (Figs. 3A and 3B), while the KD value for WT IDH1 was noticeably higher, over 50 μmol/L (Fig. 3C). The result is similar to the IDH1-R132H/C IC_{50} and WT IDH1 IC_{50} value, suggesting that DC_H31 is a potential selective inhibitor to bind IDH1-R132H/C directly.

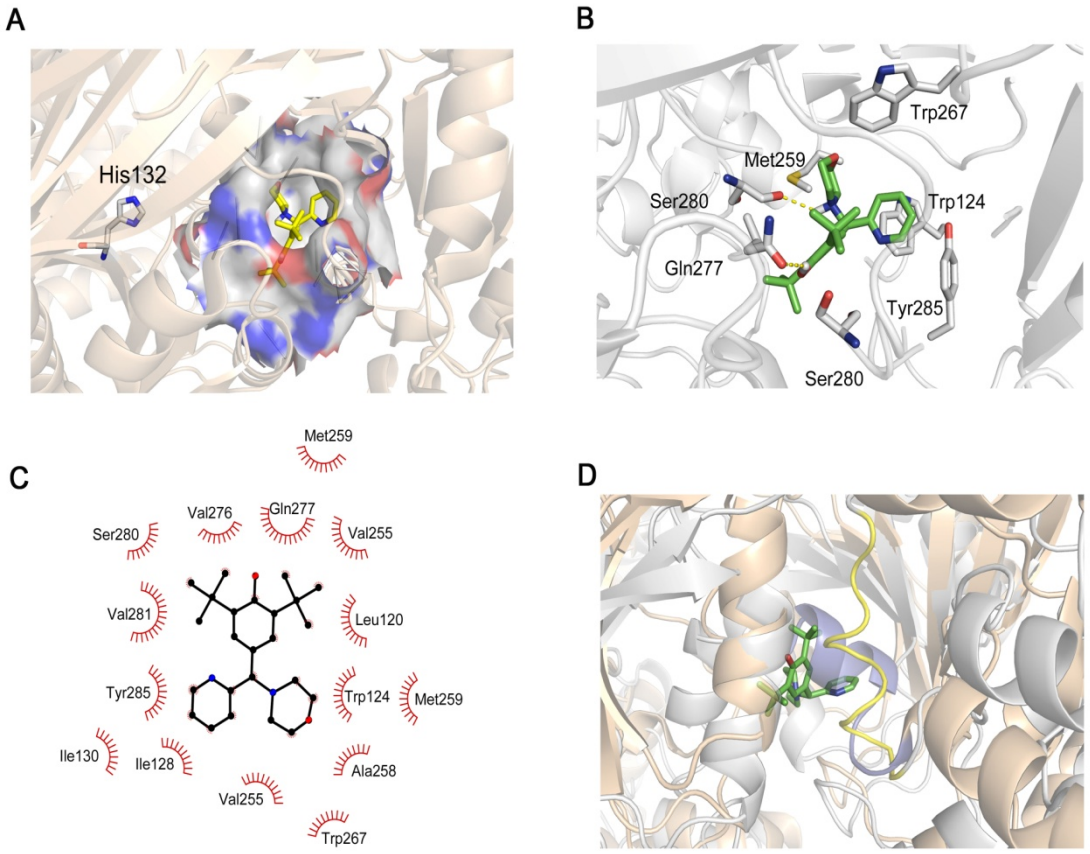

Figure4. Putative binding mode between DC_H31 and IDH1-R132H. A) Overview of the allosteric binding pocket between the two monomers. H132 is shown as gray sticks. **B)** Detailed view of the allosteric binding pocket for DC_H31 (green). Hydrogen bonds (yellow) are indicated by yellow dotted line. **C)** Schematic diagram showing predicted interactions between IDH1-R132H and DC_H31. DC_H31 is colored in purple. Hydrophobic interactions are plotted in red arcs. **D)** Overlay of one monomer of the IDH1-R132H (gray) bound to DC_H31 (green) and the WT IDH1 (wheat). Regulatory segment in IDH1-R132H and WT IDH1 is depicted in yellow and lavender respectively.

The selective and effective inhibitory activity of DC_H31 against IDH1-R132H/C prompted

us to disclose the molecular mechanism of the inhibitory activity of DC_H31. Molecular docking study was employed to reveal the binding mode and structural details of its interactions with mutant IDH1. The crystal structures of IDH1-R132H (PDB ID: 5LGE)[28] were selected and a putative binding mode was generated by Glide program with XP mode of the maestro. The results suggested that DC_H31 occupied the allosteric pocket between the two monomers far away from the mutation site with 12.6 Å. (Fig. 4A.). The binding site is also not located at the active site, Tyr139, because of highly polarity as defined by the amino acids lining the site [29]. The allosteric pocket lined on three sides by Tyr285, Trp124, Met259, Trp267, and the remaining side was formed by residues in a regulatory segment such as Ser280, Gln277[30](Fig.4B.). An assumption was proposed that DC_H31 inhibits the IDH1-R132H enzyme function through an allosteric mechanism of inhibition.

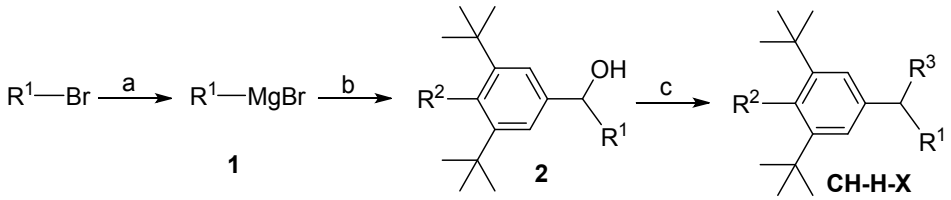

Scheme 1. Synthesis of the compounds CH-H-X. Conditions and reagents: (a) R^1Br, Mg, I_2, THF, 30 °C; (b) 3,5-di-tert-butyl-4-hydroxybenzaldehyde or 3,5-di-tert-butylbenzaldehyde, 30 °C, two steps: 65-70% yields; (c)1) MsCl, CH_2Cl_2, rt; 2) R^3XH (X = N; O; S), DMF,80-90 °C, two steps: 50-70% yields.

We next synthesized a series of derivatives(Scheme.1) and evaluated the structure-activity relationships (SAR) of DC_H31 and its derivatives based on the results of biochemistry assay to validate the scaffold authenticity of DC_H31. DC_H31 formed two hydrogen bond to the carbonyl group of Gln277 and hydroxyl group Ser280 respectively. The hydroxyl in the scaffold of DC_H31 formed a hydrogen bond to the carbonyl group of Gln277, which may clearly explain the different inhibitory activity between DC_H31 and CH-H-16 or CH-H-17. Inhibitory activity totally disappeared when the hydroxyl was moved from DC_H31. Another hydrogen bond was observed between nitrogen atom of morpholine group and Ser280. Obviously, the hydrogen bond is vital to the inhibitory activity, which accounts for the huge difference in inhibitory activity between CH-H-3, CH-H-4 and DC_H31. However, the oxygen atom at the morpholine group had less importance, and the activity was no much change when the oxygen atom was replaced by a nitrogenous group (CH-H-2). However, the activity gradually decreased when the nitrogenous

group was linked with various lengths of chains because of the steric hindrance, such as compounds CH-H-5 to CH-H-11.

Besides polar interactions as mentioned above, a highly hydrophobic environment surrounded by the allosteric pocket may contribute to stabilize the DC_H31 conformation in the pocket. In addition, it should be noticed that the pyridine group of the molecular forms three edge-to-face interaction with Trp124, Tyr285, Trp267 in three different directions respectively and is stabilized by powerful hydrophobic forces around the pocket (Fig. 4C). In addition, any chemical modifications on this group could reduce the inhibitory activity. It is clear that the pyridine group plays a crucial role to the improvement in inhibitory activity, which clarifies the molecular mechanism for better inhibitory activity of DC_H31 compared to its analogues (CH-H12, CH-H13, and CH-H14).

Table 1. Structures and biochemical IC_{50} (μmol/L) data for DC_H31 and its analogues.

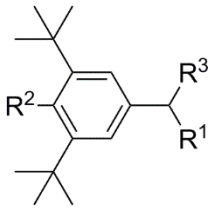

Compounds.	R^1	R^2	R^3	Biochemical IC_{50}(μmol/L)		
				IDH1-R132H	IDH1-R132C	WT IDH1
CH-H-1	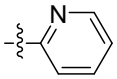	**OH**	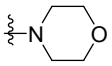	0.41	2.7	43.7
CH-H-2	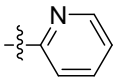	**OH**	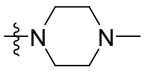	3.0	4.9	~50
CH-H-3	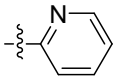	**OH**	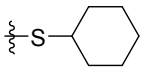	>50	>50	>50
CH-H-4	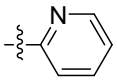	**OH**	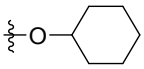	>50	>50	>50
CH-H-5	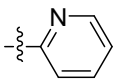	**OH**	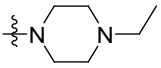	12	4.8	6.4

CH-H-6	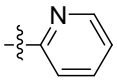	**OH**	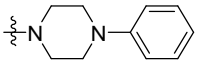	>50	>50	>50
CH-H-7	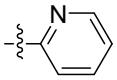	**OH**	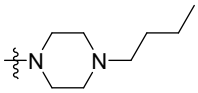	>50	9	12.79
CH-H-8	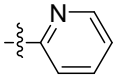	**OH**	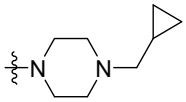	>50	18	31
CH-H-9	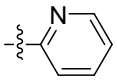	**OH**	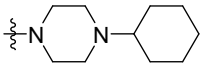	>50	>50	>50
CH-H-10	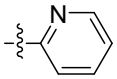	**OH**	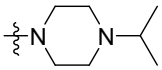	4.76	7	3
CH-H-11	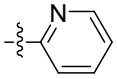	**OH**	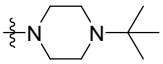	>50	9	8.5
CH-H-12	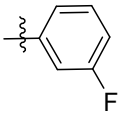	**OH**	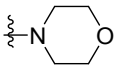	>50	>50	>50
CH-H-13	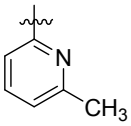	**OH**	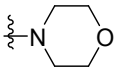	>50	>50	>50
CH-H-14	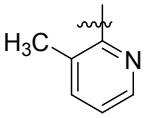	**OH**	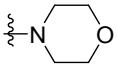	20	4.7	0.8
CH-H-15	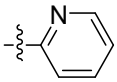	**H**	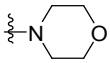	>50	>50	>50
CH-H-16	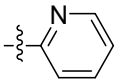	**H**	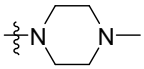	>50	>50	>50

Note: The IC_{50} values for IDH1-R132H and IDH1-R132C and WT IDH1 are the mean of three determinations performed as described method.

When the IDH1-R132H:DC_H31 conformation was overlaid to the WT IDH1 structure (PDB: 1T09) [31], we found the α10 regulatory segment (seg-2), a partially α-helix structure, in WT IDH1 conformation blocked the homologous allosteric site which was bound by DC_H31 in IDH1-R132H (Fig. 4D). In the WT IDH1 structures, Arg132 formed an ionic interaction with Asn271 of the seg-2, whereas the ionic interaction did not produce because of the mutation of Arg

to His in IDH1-R132H [6, 31]. Destabilization of seg-2 due to the lacking of the R132:N271 interaction may afford DC_H31 have access to the allosteric site of IDH1-R132H achieving mutant selectivity. Taken together, mutant selectivity for IDH1 is achieved by the intrinsic lability of regulatory segment in IDH1-R132H compared to WT IDH1. However, we need further confirmation to verify that the long distance between H132 to the allosteric pocket is the reason for the pan-inhibitory activity.

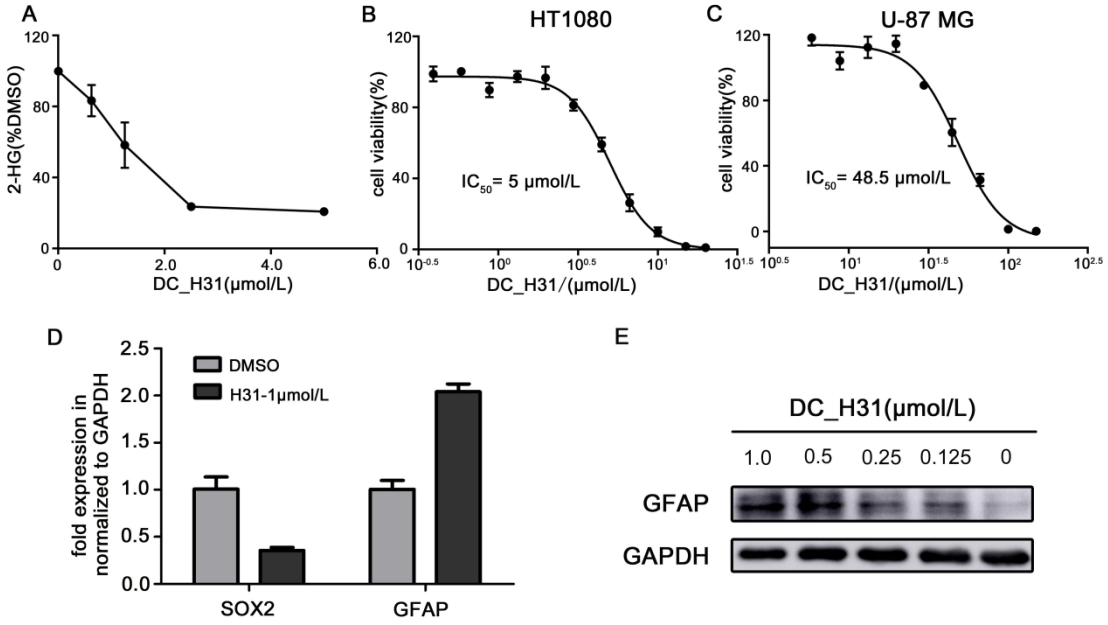

Figure5. **DC_H31 decreases intracellular 2-HG production and affects cell proliferation and differentiation.** **A)** DC_H31 inhibits intracellular 2-HG production in HT1080 cells within 48h. **B)** And **C)** DC_31 inhibits HT1080 cell proliferation but have weak effect on U87-MG. **D)** qRT-PCR results of Sox2 and GFAP expression in HT1080 cells treatment with DC_H31 after 6 days. **E)** DC_H31 increases expression of GFAP and promotes HT1080 cell differentiation in the presence of DC_H31 for 6 days. (Error bar are mean ±S.D. for three replicates)

As HT1080 cells produced the high level of 2-HG due to the neomorphic enzyme function of the missense mutation in IDH1, to further demonstrate the inhibition of IDH1 mutation in cells by DC_H31, the 2-HG assay was carried out with 0.625 μmol/L, 1.25 μmol/L, 2.5 μmol/L, 5 μmol/L DC_H31[6]. As shown in the figure 5A, 2-HG levels declined to half of DMSO control when DC_H31 concentration up to 1.25 μmol/L, and measurements of 2-HG production in a culture medium of HT1080 cells demonstrated dose-dependent inhibition after 48h of treatment.

As mentioned above, inhibiting the mutation could affect cells proliferation. HT1080 cell line harboring IDH1-R132C mutation and U-87 MG cell line, a WT IDH1 cell, were chosen for the

cell proliferation assay to evaluate the cellular activity of DC_H31. As shown in figure 5B and 5C, inhibition of HT1080 cell proliferation was observed in a dose-dependent manner after 72h treatment with a range of concentrations of DC_H31. The compound could inhibit HT1080 cells growth with the IC_{50} value of 5 μmol/L while the minimal effect on the proliferation of U-87 MG cells was seen with the IC_{50} value of 48.7 μmol/L. Noticeably, HT1080 cells were more sensitive to inhibition by DC_H31 than U-87 MG cells, at the nearly 10-fold difference between the two cell lines.

Furthermore, in order to determine whether DC_H31 could induce differentiation in HT1080 cells, SRY-box2 (SOX2) and glial fibrillary acidic protein (GFAP) which are used to indicate the degree of differentiation of HT1080[32] were selected to determine the inhibition of DC_H31 against the transcription of IDH1-R132C downstream genes. After the treatment with 1 μmol/L DC_H31 or DMSO for 6 days, quantitative fluorescence real-time PCR (qRT-PCR) was used to measure the transcription of the two genes in HT1080 cells. As shown in Fig. 5D, DC_H31 could inhibit the transcription of SOX2 genes and upregulate the transcription of GFAP genes. Meanwhile, western blot assay was performed to evaluate the alteration of the protein GFAP. As shown in Fig. 5E, treatment with 0.5 μmol/L DC_H31 induced the expression of GFAP compared to DMSO control, confirming the inhibitory activity of DC_H31 with on-target behavior.

IDH1–R132H/C are highly attractive targets for the treatment of gliomas and AML. Although many IDH inhibitors have been discovered since the first report in 2012, there is still pressing need to develop novel pan-inhibitors for IDH1-R132H/C. In this study, we identified a small molecular, DC_H31, that could potentially inhibit both IDH1-R132H and IDH1-R132C with an IC_{50} value of 0.41 μmol/L and 2.7 μmol/L respectively. At the cellular level, DC_H31 effectively inhibited the proliferation of HT1080 cells and was capable of reducing 2-HG levels in the HT1080 cell line. In addition, the transcription of mutant IDH1 downstream genes was altered by DC_H31, and the protein abundance of GFAP also increased which validated inhibitory activity of this compound. Molecular docking studies revealed the potential binding mechanism of DC_H31 with IDH1-R132H and facilitated to discovery better mutant IDH1 inhibitors. Overall, these results demonstrate that DC_H31 deserves further structure optimization as a pan-inhibitor of IDH1-R132H and IDH1-R132C for their potential use in the chemotherapeutics of patients with IDH1-mutant gliomas and AML.

Acknowledgements

Funding: This work was funded by Large-scale Protein Preparation System at the National Facility for Protein Science in Shanghai (NFPS), Zhanjiang Lab, and China for providing technical support and assistance in data collection and analysis. We gratefully acknowledge financial support from the National Natural Science Foundation of China (21472208, 81625022, and 81430084 to C.L.); K.C. Wong Education Foundation to C.L., Chinese Academy of Sciences (XDA12020353 and XDA12050401) and China Postdoctoral Science Foundation (2017M621571 to L.Y.).

Author Contributions

Cheng Luo, Mingqian Feng, Zhe Duan and Jingqiu Liu designed the study, Zhe Duan and Jingqiu Liu performed the assays, Hua Chen and Liping Niu instructed the chemical synthesis including DC_H31 and the derivatives, Jun Wang performed molecular docking analysis**,** Zhe Duan and Jingqiu Liu analyzed data wrote the manuscript with input from all of the authors.

References:

1 Reitman ZJ, Hai Y. Isocitrate dehydrogenase 1 and 2 mutations in cancer: alterations at a crossroads of cellular metabolism.. Cancerspectrum Knowledge Environment 2010; 102 (13): 932-41.

2 Turkalp Z, Karamchandani J, Das S. IDH mutation in glioma: new insights and promises for the future. JAMA NEUROL 2014; 71 (10): 1319.

3 Popovici-Muller J, Saunders JO, Salituro FG, Travins JM, Yan S, Zhao F*, et al.*. Discovery of the First Potent Inhibitors of Mutant IDH1 That Lower Tumor 2-HG in Vivo. ACS MED CHEM LETT 2012; 3 (10): 850.

4 Yan H, Parsons DW, Jin G, McLendon R, Rasheed BA, Yuan W*, et al.*. IDH1 and IDH2 mutations in gliomas [Journal Article; Research Support, N.I.H., Extramural; Research Support, Non-U.S. Gov't]. N Engl J Med 2009; 360 (8): 765-73. eng.

5 Molenaar RJ, Radivoyevitch T, Maciejewski JP, Noorden CJFV, Bleeker FE. The driver and passenger effects of isocitrate dehydrogenase 1 and 2 mutations in oncogenesis and survival prolongation. Biochimica et Biophysica Acta (BBA) - Reviews on Cancer 2014; 1846 (2): 326-41.

6 Lenny D, White DW, Stefan G, Bennett BD, Bittinger MA, Driggers EM*, et al.*. Cancer-associated IDH1 mutations produce 2-hydroxyglutarate. NATURE 2010.

7 Dinardo CD, Propert KJ, Loren AW, Elisabeth P, Zhuoxin S, Levine RL*, et al.*. Serum 2-hydroxyglutarate levels predict isocitrate dehydrogenase mutations and clinical outcome in acute myeloid leukemia. BLOOD 2013; 121 (24): 4917-24.

8 Peppi K, Sungwoo L, Duncan CG, Giselle L, Gang L, Shakti R*, et al.*. Transformation by the (R)-enantiomer of 2-hydroxyglutarate linked to EGLN activation. NATURE 2012; 483 (7390): 484-88.

9 Xu W, Yang H, Liu Y, Yang Y, Wang P, Kim SH*, et al.*. Oncometabolite 2-hydroxyglutarate is a competitive inhibitor of alpha-ketoglutarate-dependent dioxygenases [Journal Article; Research Support, N.I.H., Extramural; Research Support, Non-U.S. Gov't]. CANCER CELL 2011; 19 (1): 17-30. eng.

10 Stefan G, Cairns RA, Minden MD, Driggers EM, Bittinger MA, Hyun Gyung J*, et al.*. Cancer-associated metabolite 2-hydroxyglutarate accumulates in acute myelogenous leukemia with isocitrate dehydrogenase 1 and 2 mutations.. J EXP MED 2010; 207 (2): 339-44.

11 Fathi AT, Hossein S, Borger DR, Ballen KK, Amrein PC, Attar EC*, et al.*. Prospective serial evaluation of 2-hydroxyglutarate, during treatment of newly diagnosed acute myeloid leukemia, to assess disease activity and therapeutic response. BLOOD 2012; 120 (23): 4649-52.

12 Leopold S, David C, Jochen M, Claus-Dieter L, Christine-Maria H, Heike P*, et al.*. Increased levels of 2-hydroxyglutarate in AML patients with IDH1-R132H and IDH2-R140Q mutations. EUR J HAEMATOL 2010; 85 (5): 457-59.

13 Maxime J, Elena M, Véronique S, Jean-Baptiste M, Aline R, Cyril Q*, et al.*. Serum 2-hydroxyglutarate production in IDH1- and IDH2-mutated de novo acute myeloid leukemia: a study by the Acute Leukemia French Association group. J CLIN ONCOL 2014; 32 (4): 297-305.

14 Borger DR, Lipika G, Thomas Y, Poon RT, Marek A, Vikram D*, et al.*. Circulating oncometabolite 2-hydroxyglutarate is a potential surrogate biomarker in patients with isocitrate dehydrogenase-mutant intrahepatic cholangiocarcinoma. CLIN CANCER RES 2014; 20 (7): 1884-90.

15 Wiseman DH, Small HF, Wilks DP, Waddell ID, Dennis MW, Ogilvie DJ*, et al.*. Elevated plasma 2-hydroxyglutarate in acute myeloid leukaemia: association with the IDH1 SNP rs11554137 and severe

renal impairment. BRIT J HAEMATOL 2014; 166 (1): 145-48.
16 Hodges TR, Choi BD, Bigner DD, Hai Y, Sampson JH. Isocitrate dehydrogenase 1: what it means to the neurosurgeon: a review. J NEUROSURG 2013; 118 (6): 1176-80.
17 Dan R, Janeta PM, Nicolaos P, Sevin T, Christian G, Carl C*, et al.*. An inhibitor of mutant IDH1 delays growth and promotes differentiation of glioma cells. SCIENCE 2013; 340 (6132): 626-30.
18 Fang W, Jeremy T, Byron DL, Virginie PL, Stefanie S, Erica H*, et al.*. Targeted inhibition of mutant IDH2 in leukemia cells induces cellular differentiation. SCIENCE 2013; 340 (6132): 622-26.
19 Theresa S, Lukas B, Stefan P, Felix S, Benedikt W, Jasmin Q*, et al.*. A vaccine targeting mutant IDH1 induces antitumour immunity. NATURE 2014; 512 (7514): 324-27.
20 Adnan E, Ippolito JE, Lynne C, Jan C, Jayne M, David PW. A high-throughput fluorimetric assay for 2-hydroxyglutarate identifies Zaprinast as a glutaminase inhibitor. CANCER DISCOV 2014; 4 (7): 828-39.
21 Souba WW. Glutamine and cancer. ANN SURG 1993; 218 (6): 715-28.
22 Sevin T, Fabius AWM, Alexandra B, Alicia P, Cameron B, Jason H*, et al.*. Efficient induction of differentiation and growth inhibition in IDH1 mutant glioma cells by the DNMT Inhibitor Decitabine. Oncotarget 2013; 4 (10): 1729-36.
23 Alexandra B, Vafi S, Sevin T, Fabius AWM, Baia GS, Eberhart CG*, et al.*. 5-azacytidine reduces methylation, promotes differentiation and induces tumor regression in a patient-derived IDH1 mutant glioma xenograft. Oncotarget 2013; 4 (10): 1737-47.
24 Popovicimuller J, Lemieux RM, Artin E, Saunders JO, Salituro FG, Travins J*, et al.*. Discovery of AG-120 (Ivosidenib): A First-in-Class Mutant IDH1 Inhibitor for the Treatment of IDH1 Mutant Cancers. ACS MED CHEM LETT 2018; 9 (4): 300-05.
25 Theresa S, Lukas B, Stefan P, Felix S, Benedikt W, Jasmin Q*, et al.*. A vaccine targeting mutant IDH1 induces antitumour immunity. NATURE 2014; 512 (7514): 324-27.
26 Okoye-Okafor UC, Bartholdy B, Cartier J, Gao EN, Pietrak B, Rendina AR*, et al.*. New IDH1 mutant inhibitors for treatment of acute myeloid leukemia. NAT CHEM BIOL 2015; 11 (11): 878-86.
27 Myszka DG. KINETIC ANALYSIS OF MACROMOLECULAR INTERACTIONS USING SURFACE PLASMON RESONANCE BIOSENSORS. Curr Opin Biotechnol 1997; 8 (1): 50-57.
28 Pusch S, Krausert S, Fischer V, Balss J, Ott M, Schrimpf D*, et al.*. Pan-mutant IDH1 inhibitor BAY 1436032 for effective treatment of IDH1 mutant astrocytoma in vivo. ACTA NEUROPATHOL 2017; 133 (4): 629-44.
29 Levell JR, Caferro T, Chenail G, Dix I, Dooley J, Firestone B*, et al.*. Optimization of 3-Pyrimidin-4-yl-oxazolidin-2-ones as Allosteric and Mutant Specific Inhibitors of IDH1. ACS MED CHEM LETT 2017; 8 (2): 151.
30 Yang, Chen, Zhong, Yingjie, Peng, Zheng*, et al.*. Molecular mechanisms of " off-on switch " of activities of human IDH1 by tumor-associated mutation R132H. CELL RES 2010; 20 (11): 1188-200.
31 Xiang X, Jingyue Z, Zhen X, Baozhen P, Qiuhua H, Eddy A*, et al.*. Structures of human cytosolic NADP-dependent isocitrate dehydrogenase reveal a novel self-regulatory mechanism of activity. J BIOL CHEM 2004; 279 (32): 33946.
32 Hsieh JK, Hong CS, Manjila S, Cohen ML, Lo S, Rogers L*, et al.*. An IDH1-mutated primary gliosarcoma: case report. J NEUROSURG 2016; 126 (2): 1-05.
33 Zhang JH, Chung TDY, Oldenburg KR. A Simple Statistical Parameter for Use in Evaluation and Validation of High Throughput Screening Assays. J BIOMOL SCREEN 1999; 4 (2): 67-73.

34 Smith PK, Krohn RI, Hermanson GT, Mallia AK, Gartner FH, Provenzano MD*, et al.*. Measurement of protein using bicinchoninic acid. ANAL BIOCHEM 1985; 150 (1): 76-85.

35 Tian L, Hu J, Lu W, Jie H, Hong D, Hao J*, et al.*. Identification of small molecule inhibitors targeting the SMARCA2 bromodomain from a high-throughput screening assay. ACTA PHARMACOL SIN 2018; 39 (9).

Supplementary Materials for

Discovery of DC_H31 as Potential mutant IDH1 Inhibitor through NADPH-based High Throughput Screening

Zhe Duan[a], Jingqiu Liu[b], Liping Niu[c], Jun Wang [b], Mingqian Feng[a*], Hua Chen [c*], Cheng Luo[b*]

a College of Life Science and Technology, Huazhong Agricultural University, Wuhan 430070, China

b State Key Laboratory of Drug Research, Shanghai Institute of Materia Medica, Chinese Academy of Sciences, Shanghai 201203 P. R. China

c Key Laboratory of Chemical Biology of Hebei Province, College of Chemistry and Environmental Science, Hebei University, Bao ding 071002, China

These authors contributed equally: Zhe Duan and Jingqiu Liu

[*]Corresponding authors

fengmingqian@mail.hzau.edu.cn

Cheng Luo: cluo@simm.ac.cn

Hua Chen: hua-todd@163.com

Materials and methods

Protein expression and purification

Proteins were over expressed in bacterial systems and purified by affinity chromatography. The WT IDH1 insert was amplified by standard PCR procedure and ligated to the pET28a vector using CloneExpress One Step Cloning Kit (Vazyme). The correct construct was verified by Sanger sequencing. Based on the WT IDH1 plasmid, the IDH1-R132H/C was obtained using the site-directed mutagenesis kit .

The plasmids were transformed into BL21 cells for over expressing the fusion protein with an N-terminal 6×His-tag. (Both competent cell purchased from TRANSGEN BIOTECH). The transformed BL21 cells were cultured in LB media containing 50 μg/ml kanamycin, 0.4 mmol/L isotropy-β-D-thiogalactoside at 16°C for 13-15 hours, then collected and sonicated in pre-cooled lysis buffer (20 mmol/L Tris-HCl pH 7.5, 150 mmol/L NaCl, 1 mmol/L β-ME and 20 mmol/L imidazole). Cell debris were centrifuged at 18,000 rpm for 1 hours at 4℃. The supernatant was loaded on 5 ml HisTrap HP, Superdex 75 10/300 column (GE Healthcare). Purified proteins were stored at −80°C.

Compound library

A compound library containing 2, 5000 compounds of diverse structures was purchased from the SPECS Company (SPECS_SC_10mg_ Dec2016). AGI-5198, serving as a positive control [17], was purchased from MCE. The purity of all compounds is greater than 95% (LCMS). All compounds were dissolved in Dimethyl sulfoxide (DMSO) and stored in 4 °C for a long time.

High-throughput screening with enzyme activity assay

Mutant IDH1 catalyzed the conversion of α-KG to 2-HG accompanied by NADPH consumption, and the inhibition of IDH1-R132H/C enzyme activity by small molecule was evaluated by a fluorescent assays of NADPH depletion to identify lead compounds. In the assay, the remaining NADPH, which is inversely proportional to IDH1-R132H/C activity, was measured at the endpoint of the reaction by a fluorescent reader (BMG POLARstar omega, λex = 355nm, λem = 460nm).

Compounds were prepared in 100% DMSO as 10mM stock and diluted 1:1000 into the final reaction of the first screen. The positive control drug was also prepared as 10 mmol/L stock in DMSO. The enzyme reactions were performed in 384-well plates at room temperature containing 1X assay buffer (20 mmol/L Tris, pH 7.5, 150 mmol/L NaCl, 5 mmol/L MgCl2), 10 μmol/L NADPH, 2.5 mmol/L αKG and 100nmol/L IDH1-R132H enzyme or 20 nmol/L IDH1-R132C enzyme, and plates were incubated at room temperature for 40 minutes in a final volume of 50 μl. The wild type enzyme reactions were also performed in 384-well plate under the same conditions but contain 10μmol/L NADP+, 5mmol/L isocitrate and 60 nmol/L IDH1 enzyme.

This assay was also used to determine DC_H31 which was prepared with a dose-response curve starting with 50 μmol/L in seven dilution steps in IDH1-R132H/C test and starting with 150 μmol/L in five dilution steps in wild type IDH1 assay. The relative fluorescence versus inhibitor concentration was proportional.

Z′ factor and S/B calculation

The Z' factor, as a parameter of the high-throughput screen assay [33], was calculated to

evaluate the reliability of the test methods as the below formula:

$$Z'=1-(3*(\delta p+\delta n) /|\mu n-\mu p|)$$

In this formula, μp, δp, μn and δn were used for the means and standard deviations of the positive (p) and negative (n) controls respectively. The reaction adding DMSO was employed as negative control and lacking of mutation protein in the action was positive control. The S/B value was the result of the mean of the negative controls over the mean of the positive controls in the biochemical reactions.

Surface Plasmon Resonance (SPR)-based binding assays

SPR is an efficient method for measuring interactions between small molecule and protein [27]. In this study, we applied SPR to measure the interactions between the newly discovered DC_H31 towards IDH1-R132H/C and WT IDH1. The SPR-based binding assay was performed with HBS buffer (10 mmol/L HEPES pH 7.4, 150 mmol/L NaCl, and 0.1% (v/v) DMSO) on GE Healthcare Biacore T200 instrument at 25 °C. IDH1-R132H, IDH1-R132C and WT IDH1 were diluted in 10 mmol/L sodium acetate, and covalently immobilized on the CM5 sensor chip respectively by the standard amine-coupling procedure. The test compound DC_H31 was serially diluted to a concentration range between 25 μmol/L to 0.78 μmol/L with HBS buffer in IDH1-R132H/C test, or between 50 μmol/L to 1.56 μmol/L in WT IDH1 test, and injected into the chip at 30 μL/min rate. The combination step was set at 120 s, following 150 s dissociation step. The KD value of DC_H31 was calculated by the state model of Biacore T200 evaluation software.

Cell culture and viability assays

The sarcoma cell line HT1080, featuring an endogenous IDH1-R132C mutation, and likely glioblastoma cell line U-87 MG were both purchased from American Type Culture Collection (ATCC) and maintained in DMEM medium with 10% fetal bovine serum supplement and 1% penicillin and streptomycin antibiotic (Gibco® Invitrogen, Carlsbad, USA) under standard culture conditions (37 °C, 5% CO2).

For cell viability assay, the two cell lines were seeded into 96-well plates. After attachment to the culture plate, the cells were treated with a range of concentrations of compounds for 72 h in triplicate, and the same concentration of DMSO was employed as negative control. The fraction of viable cells was estimated through Cell Titer-Glo luminescent assays using multilabel reader (Envision, PerkinElmer). All data were analyzed by GraphPad Prism 5.0 software and fitted to nonlinear curve to calculate IC_{50} value.

Western Blot

HT1080 cells were cultured in 6-well plate at the appropriate density and treated with indicated concentrations of DC_H31 or DMSO control for 6 days after cell attachment. Treated HT1080 cells was collected and lysed by cell lysis buffer. Then, protein samples quantified by BCA protein determination method [34] were separated by 12% SDS-polyacrylamide gradient gel and transferred to nitrocellulose membranes. The membranes were blocked in 5% (w/v) nonfat milk for 1h and then incubated with anti-GFAP and anti-GAPDH primary antibodies at 4 ℃ overnight. Subsequently, after washed by TBST three times, the membranes were incubated with HRP-conjugated anti-mouse or anti-rabbit secondary antibody for 2h and detected in ChemiScope3400 imaging system using ECL substrate.

Quantitative RT-PCR

For the q-PCR analysis assay, HT1080 cells were also cultured in 6-well plates and treated with 1 μmol/L DC_H31 or DMSO control for 6 days. Treated cells then were collected and lysed for RNA extraction using the Trizol Reagent kit. After that, previous RNA was reverse transcripted for Real-time PCR analysis on the Quant Studio 6 Flex Real-Time PCR system using the SYBR Green Real-Time PCR Master Mix. Data were visualized with the expression value for SOX2 gene and GFAP gene in the DMSO control or treated samples.

Measurement of 2-HG

The level of 2-Hydroxyglutarate(2-HG) was quantified in HT1080 cells in the absence or presence of DC_H31 compound by LC/MS. Firstly, HT1080 cells were seeded into a 6-well plate. After attaching to plate, cells received DC_H31 with various concentrations and received the same concentration of DMSO as a negative control in complete medium for 48 h. Cell culture medium was then harvested for 2-HG extraction and measured by LC/MS using DIONEX UltiMate 3000 and Thermo Fisher Scientific TSQ Quantiva. A Calibration curve was done by deterring a standard 2-HG dissolved in 80:20 methanol: water. LC was performed on Waters XSELECT HSS T3analytical column. The metabolite 2-HG and the standard 2-HG was monitored by the transition of 147.0 m/z > 101.1 m/z and 51.2 m/z using a DP −35.0, collision energy −16.0, and CXP −9.0. Data were acquired and analyzed with Thermo Xcalibur3.0.63. The peak areas of the metabolite 2-HG were normalized by the peak area of the standard 2-HG. The value of 2-HG concentration was normalized to the DMSO negative control and expressed as percentages of negative control activity [6].

Binding mode analysis

Molecular docking experiments were performed to analyze the possible binding modes of DC_H31 using the molecular modeling software Maestro (Schrödinger, LLC: New York, NY, 2009) [35]. Firstly, the structure of DC_H31 was drawn using Chem3D and prepared by LigPrep and Advanced Conformational Search to generate different protonation states and conformations with the OPLS3 force field. Then the crystal structure of IDH1-R132H selected from the protein data bank (PDB code: 5LGE) was optimized as molecular docking receptor through the Protein preparation Wizard module in Maestro with a pH value of 7.0. In addition, a 20 Å × 20 Å × 20 Å receptor grid box centered at the BAY 1436032 binding center was generated in the Receptor Grid Generation Module. Other parameters were set as default. Finally, Glide extra-precision (XP) mode of induced-fit docking was used to dock the prepared ligand molecular into the defined binding site with standard protocols. After Glide docking, the binding mode of the ligand was chosen according to the score.

Chemistry

Column chromatography was carried out on flash silica gel (300-400 mesh). TLC analysis was conducted on silica gel plates (Silica G UV254). Melting points were measured in an open capillary on an SGW X-4 melting point apparatus and were uncorrected. NMR spectra were recorded at 400 MHz and 600 MHz for 1H on a Bruker instrument. Chemical shifts (δ values) and coupling constants, (J values) were given in ppm and hertz, respectively, using TMS (1HNMR) solvent as internal standard. The High Resolution Mass Spectra (HRMS) were carried out on an FTICR-MS (Ionspec 7.0T) mass spectrometer with electrospray ionization (ESI). Element analysis was performed using a Heraeus (CHNO, rapid) elemental analyzer. The silica gel (300-400 mesh) for flash column chromatography was from Qingdao Marine Chemical (China).

General procedure for the synthesis of compounds 2

A mixture of magnesium (Mg, 769 mg, 32 mmol), iodine (50 mg, 0.2 mmol) in THF (8 mL) was added slowly 6 mL of a solution of 2-bromopyridine (1.2 mL, 12.8 mmol) in THF. After the dropwise addition finished, the reaction mixture was heated at 30 °C for 2 hours. Then, 3,5-di-*tert*-butyl-4-hydroxybenzaldehyde (592 mg, 2.5mmol) was added dropwise. Their action mixture was stirred at 30°C for 24 h. After completion of the reaction by TLC, 20% ammonium chloride solution was added to quench the reaction. The mixture was extracted with dichloromethane (50 mL×3). The organic layer was washed with brine and dried over Na_2SO_4. The solid was filtered off, and the filtrate was concentrated under reduced pressure to give 2,6-di-*tert*-butyl-4-(hydroxy(pyridin-2-yl) methyl) phenol**2** (498 mg, yield 63%).

General procedure for the synthesis of compounds CH-H-X

Methane sulfonyl chloride (58 μL, 0.7 mmol) and triethylamine (238 μL) was added to a solution of compound **2** (180 mg, 0.6 mmol) in dichloromethane (5 mL) and stirred at room temperature for 1 h. After completion of the reaction by TLC, ice water was added to quench the reaction. The mixture was extracted with dichloromethane (20 mL×3). The organic layer was washed with brine and dried over Na_2SO_4. The solid was filtered off, and the filtrate was concentrated under reduced pressure to give the methylsulfonylated product (210 mg, yield 93%). To a solution of the methylsulfonylated product (210mg, 0.6 mmol) in DMF (5 mL) was added K_2CO_3 (111 mg, 0.8 mmol), morpholine (93 μL, 1.0 mmol). The mixture was stirred at 90 °C for 2 h. After completion of the reaction by TLC, The mixture was extracted with dichloromethane (20 mL×3). The organic layer was washed with brine and dried over Na_2SO_4. The solid was filtered off, and the filtrate was concentrated under reduced pressure. The residues were separated by silica gel column chromatography (V petroleum ether: V ethyl acetate = 8:1) to give CH-H-1 (108 mg, yield 53%). Under the same conditions, compounds CH-H-2 to CH-H-16 were obtained.

*2,6-di-tert-butyl-4-(morpholino(pyridin-2-yl)methyl)phenol (**CH-H-1**):*

Light yellow solid, yield 53%, m.p. 142.3-145.8 ºC; ^{1}H NMR (600 MHz, $CDCl_3$) δ(ppm): 8.51 (d, J = 4.2 Hz, 1H), 7.62 (td, J = 7.8, 1.8 Hz, 1H), 7.57 (d, J = 7.8 Hz, 1H), 7.24 (s, 2H), 7.11 – 7.09 (m, 1H), 5.11 (s, 1H), 4.30 (s, 1H), 3.75 – 3.68 (m, 4H), 2.42 (s, 2H), 2.33 (s, 2H), 1.40 (s, 18H); ^{13}C NMR (150 MHz, $CDCl_3$) δ(ppm): 162.5,

153.0, 149.1, 136.5, 135.8, 130.8, 125.0, 122.2, 121.9, 78.5, 67.1, 52.6, 34.4, 30.4; HRMS (ESI): Calcd for $C_{24}H_{34}N_2O_2Na$ ([M+Na]$^+$): 405.2518, Found: 405.2526; Anal. Calcd for $C_{24}H_{34}N_2O_2$: C, 75.35; H, 8.96; N, 7.32. Found: C, 75.43; H, 8.95; N, 7.36.

2,6-di-tert-butyl-4-((4-methylpiperazin-1-yl)(pyridin-2-yl)methyl)phenol ***(CH-H-2)****:*

White solid, yield 70%, m.p. 134.2-136.5 ^oC; ^1H NMR (600 MHz, $CDCl_3$) δ(ppm): 8.49 (d, J = 4.8 Hz, 1H), 7.60 (td, J = 8.4, 1.8 Hz, 1H), 7.55 (d, J = 7.8 Hz, 1H), 7.23 (s, 2H), 7.08 – 7.06 (m, 1H), 5.08 (s, 1H), 4.33 (s, 1H), 2.45 – 2.67 (m, 11H), 1.40 (s, 18H); ^{13}C NMR (150 MHz, $CDCl_3$) δ(ppm): 162.9, 152.8,149.0,136.4,135.7, 131.3, 125.0, 122.2, 121.7, 77.9, 55.4, 51.8, 46.0, 34.3, 30.4; HRMS (ESI): Calcd for $C_{25}H_{37}N_3ONa$ ([M+Na]$^+$): 418.2834, Found: 418.2839; Anal. Calcd for $C_{25}H_{37}N_3O$: C, 75.91; H, 9.43; N, 10.62. Found: C, 75.98; H, 9.36; N, 10.58.

2,6-di-tert-butyl-4-((cyclohexylthio)(pyridin-2-yl)methyl)phenol ***(CH-H-3)****:*

Light yellow solid, yield 52%, m.p. 101.3-102.6^oC; ^1H NMR (600 MHz, $CDCl_3$) δ(ppm): 8.53 (d, J = 4.2 Hz, 1H), 7.64 (td, J =7.8, 1.8 Hz, 1H), 7.58 (d, J = 7.8 Hz, 1H), 7.26 (s, 2H), 7.13 – 7.11 (m, 1H), 5.29 (s, 1H), 5.12 (s, 1H), 2.49 – 2.46 (m, 1H), 1.96 (d, J = 11.4 Hz, 1H), 1.83 (d, J = 11.4 Hz, 1H), 1.72 – 1.70 (m, 2H), 1.53 – 1.48 (m, 1H), 1.40 (s, 18H), 1.36-1.30 (m, 2H), 1.30 – 1.16 (m, 3H); ^{13}C NMR (150 MHz, $CDCl_3$) δ(ppm): 162.5, 152.9, 148.9, 136.7, 135.8, 131.2, 125.0, 122.6, 121.7, 54.7, 43.7, 34.4, 33.4, 30.3, 25.9, 25.8; HRMS (ESI): Calcd for $C_{26}H_{37}NOSNa$ ([M+Na]$^+$): 434.2493, Found: 434.2487; Anal. Calcd for $C_{26}H_{37}NOS$: C, 75.86; H, 9.06; N, 3.40. Found: C, 75.92; H, 9.16; N, 3.45.

2,6-di-tert-butyl-4-((cyclohexyloxy)(pyridin-2-yl)methyl)phenol ***(CH-H-4)****:*

Yellow solid, yield 67%, m.p. 112.1-113.0 ^oC; ^1H NMR (600 MHz, $CDCl_3$) δ(ppm): 8.52 (d, J = 4.6 Hz, 1H), 7.68 (t, J = 7.8 Hz, 1H), 7.59 (d, J = 7.8 Hz, 1H), 7.16 – 7.13 (m, 3H), 5.60 (s, 1H), 5.10 (s, 1H), 3.38-3.34 (m, 1H), 2.02 (d, J = 11.4 Hz, 1H), 1.89 (d, J = 11.4 Hz, 1H), 1.77 – 1.70 (m, 2H), 1.50 – 1.43 (m, 3H), 1.39 (s, 18H), 1.23 – 1.86 (m, 3H); ^{13}C NMR (150 MHz, $CDCl_3$) δ(ppm): 163.2, 153.1, 148.7, 136.6, 135.5,

132.4, 124.0, 122.0, 121.0, 81.9, 75.6, 34.3, 32.8, 32.3, 30.3, 25.8, 24.2; HRMS (ESI): Calcd for $C_{26}H_{37}NO_2Na$ ([M+Na]$^+$): 418.2722, Found: 418.2718; Anal. Calcd for $C_{26}H_{37}NO_2$: C, 78.94; H, 9.43; N, 3.54. Found: C, 78.89; H, 9.50; N, 3.62.

2,6-di-tert-butyl-4-((4-ethylpiperazin-1-yl)(pyridin-2-yl)methyl)phenol ***(CH-H-5)****:*

White solid, yield 57%, m.p. 129.5-130.5 ^oC; ^1H NMR (600 MHz, $CDCl_3$) δ(ppm): 8.49 (d, J = 4.8 Hz, 1H), 7.60 (t, J = 7.2 Hz, 1H), 7.55 (d, J = 7.8 Hz, 1H), 7.22 (s, 2H), 7.07(t, J = 6.0 Hz, 1H), 5.07 (s, 1H), 4.35 (s, 1H), 2.50 – 2.41 (m, 10H), 1.39 (s, 18H), 1.07 (t, J = 7.2 Hz, 3H); ^{13}C NMR (150 MHz, $CDCl_3$) δ(ppm): 162.8, 152.9, 149.0, 136.4, 135.7, 131.3, 125.1, 122.22, 121.7, 77.8, 53.0, 52.3, 51.6, 34.3, 30.4, 11.9; HRMS (ESI): Calcd for $C_{26}H_{39}N_3ONa$ ([M+Na]$^+$): 432.2991, Found: 432.2993; Anal. Calcd for $C_{26}H_{39}N_3O$: C, 76.24; H, 9.60; N, 10.26. Found: C, 76.31; H, 9.56; N, 10.42.

2,6-di-tert-butyl-4-((4-phenylpiperazin-1-yl)(pyridin-2-yl)methyl)phenol ***(CH-H-6)****:*

White solid, yield 52%, m.p. 101.2-102.1 ^oC; ^1H NMR (400 MHz, $CDCl_3$) δ(ppm): 8.53 (d, J = 4.8 Hz, 1H), 7.65 – 7.59 (m, 2H), 7.27 (s, 2H), 7.23(d, J = 8.8 Hz, 2H) 7.12 – 7.08 (m, 1H), 6.90 (d, J = 8.0 Hz, 2H), 6.84 (t, J = 7.2 Hz, 1H), 5.12 (s, 1H), 4.38 (s, 1H), 3.24 – 3.16 (m, 4H), 2.62 – 2.59 (m, 2H), 2.52 – 2.48 (m, 2H), 1.40 (s, 1H); ^{13}C NMR (100 MHz, $CDCl_3$) δ(ppm): 162.8, 153.0, 151.4, 149.0, 136.6, 135.8, 131.2, 129.1, 125.0, 122.2, 121.9, 77.9, 51.9, 49.2, 34.4, 30.4; HRMS (ESI): Calcd for $C_{30}H_{39}N_3ONa$ ([M+Na]$^+$): 480.2991, Found: 480.2995; Anal. Calcd for $C_{30}H_{39}N_3O$: C, 78.73; H, 8.59; N, 9.18. Found: C, 78.64; H, 8.72; N, 9.31.

2,6-di-tert-butyl-4-((4-butylpiperazin-1-yl)(pyridin-2-yl)methyl)phenol ***(CH-H-7)****:*

Light yellow solid, yield 63%, m.p. 57.8-59.2 ^oC; ^1H NMR (400 MHz, $CDCl_3$) δ(ppm): 8.49 (d, J = 4.8 Hz, 1H), 7.61-7.59 (m, 1H), 7.56 (d, J = 7.8 Hz, 1H), 7.22 (s, 2H), 7.06 (t, J =6.0 Hz, 1H), 5.07 (s, 1H), 4.34 (s, 1H), 2.46 (s, 4H), 2.39 – 2.31 (m, 4H), 1.45 (t, J = 7.8Hz, 2H), 1.40 (s, 18H), 1.33 – 1.25 (m, 4H), 0.90 (t, J = 7.2 Hz, 3H); ^{13}C NMR (100 MHz, $CDCl_3$) δ(ppm): 162.9, 152.8, 149.0, 136.4, 135.6, 131.4,

125.0, 122.2, 121.7, 77.9, 58.5, 53.5, 51.8, 34.3, 30.4, 29.0, 20.8, 14.0; HRMS (ESI): Calcd for $C_{28}H_{43}N_3ONa$ ([M+Na]$^+$): 460.3303, Found: 460.3309; Anal. Calcd for $C_{28}H_{43}N_3O$: C, 76.84; H, 9.90; N, 9.60. Found: C, 76.92; H, 9.81; N, 9.73.

2,6-di-tert-butyl-4-((4-(cyclopropylmethyl)piperazin-1-yl)(pyridin-2 yl)methyl)phenol ***(CH-H-8)****:*

Light yellow solid, yield 49%, m.p. 48.2-50.3 ^oC; ^1H NMR (400 MHz, $CDCl_3$) δ(ppm): 8.45 (d, J = 3.2Hz, 1H), 7.57 (t, J = 5.2 Hz, 1H), 7.52 (d, J = 5.2 Hz, 1H), 7.17 (s, 2H), 7.04 (t, J = 4.0 Hz, 1H), 5.04 (s, 1H), 4.30 (s, 1H), 2.59 – 2.18 (m, 10H), 1.42 (s, 18H), 0.84 – 0.79 (m, 1H), 0.44 (d, J = 5.2 Hz, 2H), 0.04 (d, J = 4.8 Hz, 2H); ^{13}C NMR (100 MHz, $CDCl_3$) δ(ppm): 162.9, 152.8, 148.9, 136.4, 135.7, 131.3, 125.0, 122.2, 121.6, 77.9, 63.8, 53.5, 51.7, 34.3, 30.4, 8.3, 3.9, 3.8; HRMS (ESI): Calcd for $C_{28}H_{41}N_3ONa$ ([M+Na]$^+$): 458.3147, Found: 458.3141; Anal. Calcd for $C_{28}H_{41}N_3O$: C, 77.20; H, 9.49; N, 9.65. Found: C, 77.08; H, 9.54; N, 9.66.

2,6-di-tert-butyl-4-((4-cyclohexylpiperazin-1-yl)(pyridin-2-yl)methyl)phenol ***(CH-H-9)****:*

Light yellow solid, yield 50%, m.p. 129.2-130.8 ^oC; ^1H NMR (400 MHz, $CDCl_3$) δ(ppm): 8.49 (d, J = 4.2 Hz, 1H), 7.60 – 7.58 (m, 1H), 7.55 (d, J = 7.8Hz,1H), 7.21 (s, 1H), 7.06 (t, J = 6.0 Hz, 2H), 5.07(s, 1H), 4.32 (s, 1H), 2.59 (s, 4H), 2.45 (s, 2H), 2.37 (s, 2H), 2.22 – 2.18 (m, 1H), 1.88 (d, J = 10.2 Hz, 2H), 1.76 (d, J = 12.0 Hz, 2H), 1.60 (d, J = 12.6 Hz, 1H), 1.39 (s, 18H), 1.26 – 1.18 (m, 2H); ^{13}C NMR (100 MHz, $CDCl_3$) δ(ppm): 162.9, 152.8, 149.0, 136.4, 135.6, 131.4, 1251, 122.2, 121.6, 77.9, 63.5, 52.3, 49.1, 34.3, 30.4, 29.0, 26.3, 25.9; HRMS (ESI): Calcd for $C_{30}H_{45}N_3ONa$ ([M+Na]$^+$): 486.3460, Found: 486.3464; Anal. Calcd for $C_{30}H_{45}N_3O$: C, 77.71; H, 9.78; N, 9.06. Found: C, 77.67; H, 9.84; N, 9.11.

2,6-di-tert-butyl-4-((4-isopropylpiperazin-1-yl)(pyridin-2-yl)methyl)phenol ***(CH-H-10)****:*

Light yellow solid, yield 67%, m.p. 137.6-138.5 ^oC;^1H NMR (400 MHz, $CDCl_3$) δ(ppm): 8.54 (d, J = 4.2 Hz, 1H), 7.68 (td, J = 7.8, 1.2 Hz, 1H), 7.41 (d, J = 7.8 Hz,

1H), 7.20 (s, 2H), 7.09 (dd, J = 6.6, 5.4 Hz, 1H), 4.36 (s, 1H), 3.40-3.35 (m, 1H), 3.16 – 3.08 (m, 4H), 2.69 (s, 2H), 2.62 (s, 2H), 1.36 (s, 18H), 1.24 (d, J = 6.0 Hz, 6H); ^{13}C NMR (100 MHz, $CDCl_3$) δ(ppm): 161.3, 153.3, 149.1, 137.1, 136.1, 130.1, 125.0, 122.6, 122.2, 76.5, 56.0, 48.9, 47.2, 34.3, 48.9, 47.2, 34.3, 30.3, 16.8, 16.7; HRMS (ESI): Calcd for $C_{27}H_{41}N_3ONa$ ([M+Na]$^+$): 446.3147, Found: 446.3143; Anal. Calcd for $C_{27}H_{41}N_3O$: C, 76.55; H, 9.76; N, 9.92. Found: C, 76.58; H, 9.80; N, 9.85.

2,6-di-tert-butyl-4-((4-(tert-butyl)piperazin-1-yl)(pyridin-2-yl)methyl)phenol ***(CH-H-11)****:*

Light yellow solid, yield 68%, m.p. 123.1-126.4 ^{o}C; ^{1}H NMR (400 MHz, $CDCl_3$) δ(ppm): 8.49 (d, J = 3.2 Hz, 1H), 7.61 – 7.56 (m, 2H), 7.20 (s, 2H), 7.07 (t, J = 4.0 Hz, 1H), 5.06 (s, 1H), 4.31 (s, 1H), 2.60 – 2.38 (m, 8H), 1.39 (s, 18H), 1.05 (s, 9H); ^{13}C NMR (100 MHz, $CDCl_3$) δ(ppm): 163.0, 152.8, 149.0, 136.4, 135.6, 131.3, 125.2, 122.2, 121.6, 78.0, 52.6, 45.8, 34.3, 30.4, 25.8; HRMS (ESI): Calcd for $C_{28}H_{43}N_3ONa$ ([M+Na]$^+$): 460.3303, Found: 460.3307; Anal. Calcd for $C_{28}H_{43}N_3O$: C, 76.84; H, 9.90; N, 9.60. Found: C, 76.88; H, 9.96; N, 9.68.

2,6-di-tert-butyl-4-((3-fluorophenyl)(morpholino)methyl)phenol ***(CH-H-12)****:*

Light yellow solid, yield 63%, m.p. 120.1-121.1 ^{o}C; ^{1}H NMR (600 MHz, $CDCl_3$) δ(ppm): 7.24 – 7.15 (m, 5H), 6.85 (t, J = 8.4 Hz, 1H), 5.09 (s, 1H), 4.10 (s, 1H), 3.73 – 3.68 (m, 4H), 2.33 (s, 4H), 1.41 (s, 18H); ^{13}C NMR (150 MHz, $CDCl_3$) δ(ppm): 163.0 (d, $^1J_{CF}$ =243.9), 152.8, 146.0, 135.8, 131.8, 129.8, 124.5, 123.5, 114.5 (d, $^2J_{CF}$ =21.3 Hz), 113.6 (d, $^3J_{CF}$ = 21.5 Hz), 76.2, 67.2, 52.5, 34.3, 30.4; HRMS (ESI): Calcd for $C_{25}H_{34}FNO_2Na$ ([M+Na]$^+$): 422.2471, Found: 422.2475; Anal. Calcd for $C_{25}H_{34}FNO_2$: C, 75.15; H, 8.58; N, 4.76. Found: C, 75.23; H, 8.65; N, 4.74.

2,6-di-tert-butyl-4-((6-methylpyridin-2-yl)(morpholino)methyl)phenol ***(CH-H-13)****:*

Light yellow solid, yield 48%, m.p. 68.5-69.3 ^{o}C; ^{1}H NMR (400 MHz, $CDCl_3$) δ(ppm): 7.50 (t, J = 7.6 Hz, 1H), 7.41 (d, J = 7.6 Hz, 1H), 7.28 (s, 2H), 6.94 (d, J =

7.6 Hz, 1H), 5.09 (s, 1H), 4.29 (s, 1H), 3.73 – 3.66 (m, 4H), 2.50 (s, 3H), 2.42 – 2.40(m, 2H), 2.33-2.30 (m, 2H), 1.40 (s, 18H); ^{13}C NMR (100 MHz, $CDCl_3$) δ(ppm): 161.9, 157.5, 152.9, 136.7, 135.7, 131.1, 125.1, 121.4, 118.9, 78.5, 67.2, 52.6, 34.4, 30.4; HRMS (ESI): Calcd for $C_{25}H_{36}N_2O_2Na$ ([M+Na]$^+$): 419.2674, Found: 419.2679; Anal. Calcd for $C_{25}H_{36}N_2O_2$: C, 75.72; H, 9.15; N, 7.06. Found: C, 75.84; H, 9.19; N, 7.13.

2,6-di-tert-butyl-4-((3-methylpyridin-2-yl)(morpholino)methyl)phenol ***(CH-H-14)****:*

Light yellow solid, yield 56%, m.p. 95.3-96.6 ^{o}C; ^{1}H NMR (400 MHz, $CDCl_3$) δ(ppm): 8.51 (d, J = 2.8Hz, 1H), 7.33 (d, J = 7.2 Hz, 1H), 7.27 (d, J = 13.2 Hz, 2H), 6.97 – 6.97 (m, 1H), 5.08 (s, 1H), 4.41 (s, 1H), 3.74 (d, J = 13.6 Hz, 4H), 2.42 (s, H), 2.37 (s, 7H) 1.38 (s, 18H); ^{13}C NMR (100 MHz, $CDCl_3$) δ(ppm): 158.9, 153.0, 147.1, 138.4, 135.5, 131.7, 129.4, 125.9, 121.4, 74.2, 66.9, 52.9, 34.3, 30.4, 29.6, 19.3; HRMS (ESI): Calcd for $C_{25}H_{36}N_2O_2Na$ ([M+Na]$^+$): 419.2674, Found: 419.2672; Anal. Calcd for $C_{25}H_{36}N_2O_2$: C, 75.72; H, 9.15; N, 7.06. Found: C, 75.77; H, 9.18; N, 7.07.

4-((3,5-di-tert-butylphenyl)(pyridin-2-yl)methyl)morpholine ***(CH-H-15)****:*

Light yellow solid, yield 73%, m.p. 93.6-94.5 ^{o}C; ^{1}H NMR (600 MHz, $CDCl_3$) δ(ppm): 8.51 (d, J = 4.2 Hz, 1H), 7.61 (td, J = 8.4, 1.8 Hz, 1H), 7.57 (d, J = 7.8 Hz, 1H), 7.33 (d, J = 1.8 Hz, 2H), 7.25 (d, J = 1.8 Hz, 2H), 7.09 – 7.07 (m, 1H), 4.38 (s, 1H), 3.76 – 3.69 (m, 4H), 2.44 – 2.34 (m, 2H), 1.29 (s, 18H); ^{13}C NMR (150 MHz, $CDCl_3$) δ(ppm): 162.1, 150.8, 149.1, 139.5, 136.5, 122.6, 122.3, 121.9, 121.2, 79.0, 67.1, 52.7, 34.8, 31.5; HRMS (ESI): Calcd for $C_{24}H_{34}N_2ONa$ ([M+Na]$^+$): 389.2569, Found: 389.2573; Anal. Calcd for $C_{24}H_{34}N_2O$: C, 78.64; H, 9.35; N, 7.64. Found: C, 78.66; H, 9.42; N, 7.67.

1-((3,5-di-tert-butylphenyl)(pyridin-2-yl)methyl)-4-methylpiperazine ***(CH-H-16)****:*

Light yellow solid, yield 78%, m.p. 97.8-98.1 ^{o}C; ^{1}H NMR (400 MHz, $CDCl_3$) δ(ppm): 8.48 (s, 1H), 7.54 (dd, J = 14.4, 7.2 Hz, 2H), 7.31 (s, 2H), 7.23 (s, 1H), 7.04 (s, 1H), 4.39 (s, 1H), 2.51 (s, 8H), 2.31 (s, 3H), 1.27 (s, 18H); ^{13}C NMR (100 MHz,

$CDCl_3$) δ(ppm): 162.4, 150.7, 149.0, 139.9, 136.4, 122.6, 122.3, 121.8, 120.9, 78.2, 55.1, 51.5, 45.6, 34.8, 31.5; HRMS (ESI): Calcd for $C_{25}H_{37}N_3Na$ ($[M+Na]^+$): 402.2885, Found: 402.2887; Anal. Calcd for $C_{25}H_{37}N_3$: C, 79.10; H, 9.82; N, 11.07. Found: C, 79.05; H, 9.86; N, 11.14.

NMR spectra

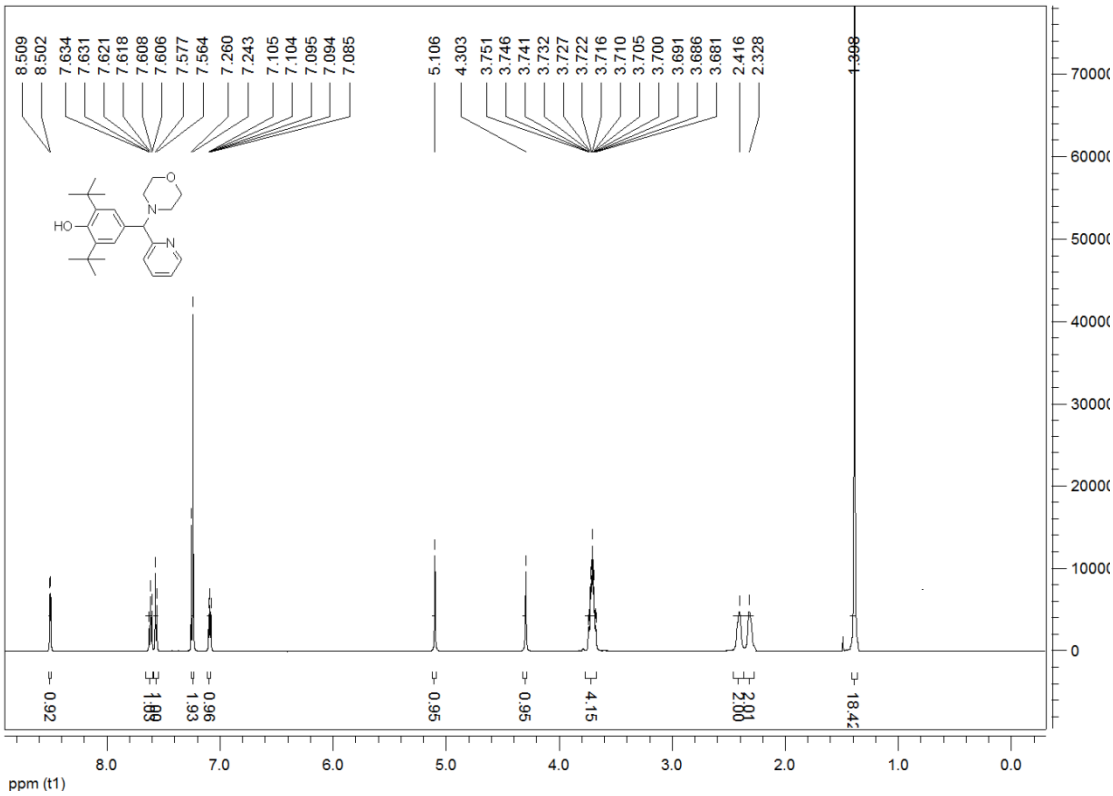

Fig.1 ^{1}H NMR of compound **CH-H-1**

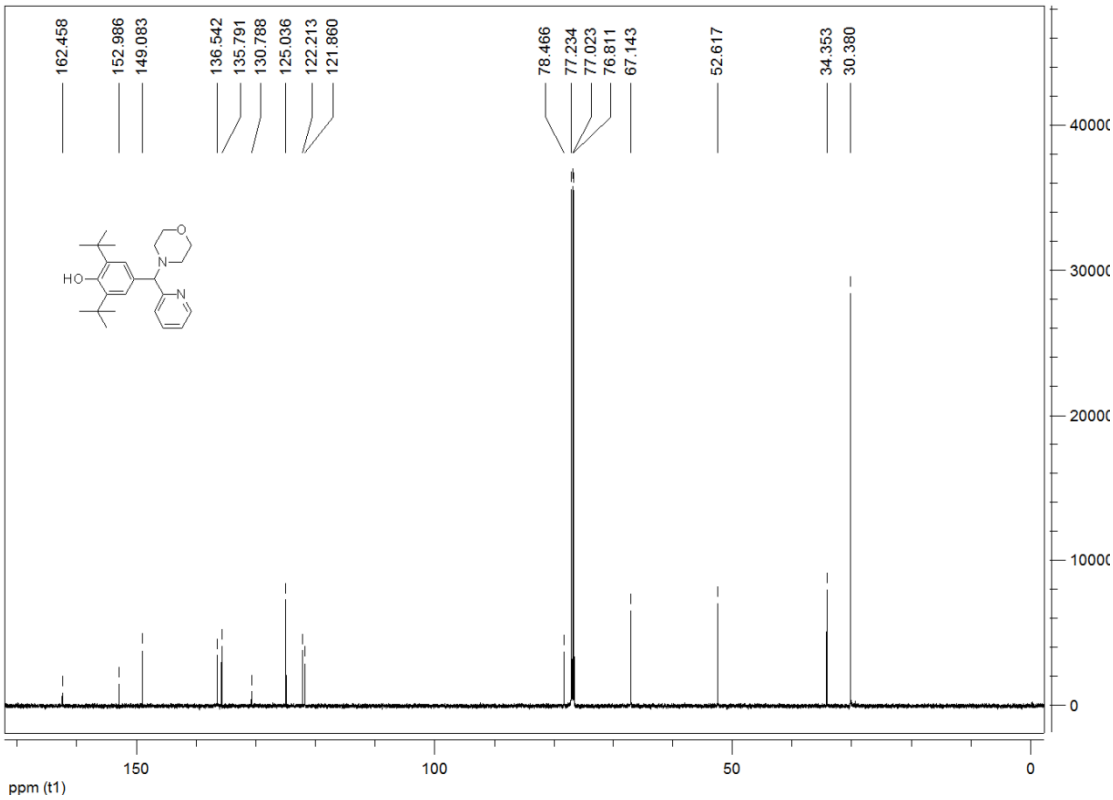

Fig.2 ^{13}C NMR of compound **CH-H-1**

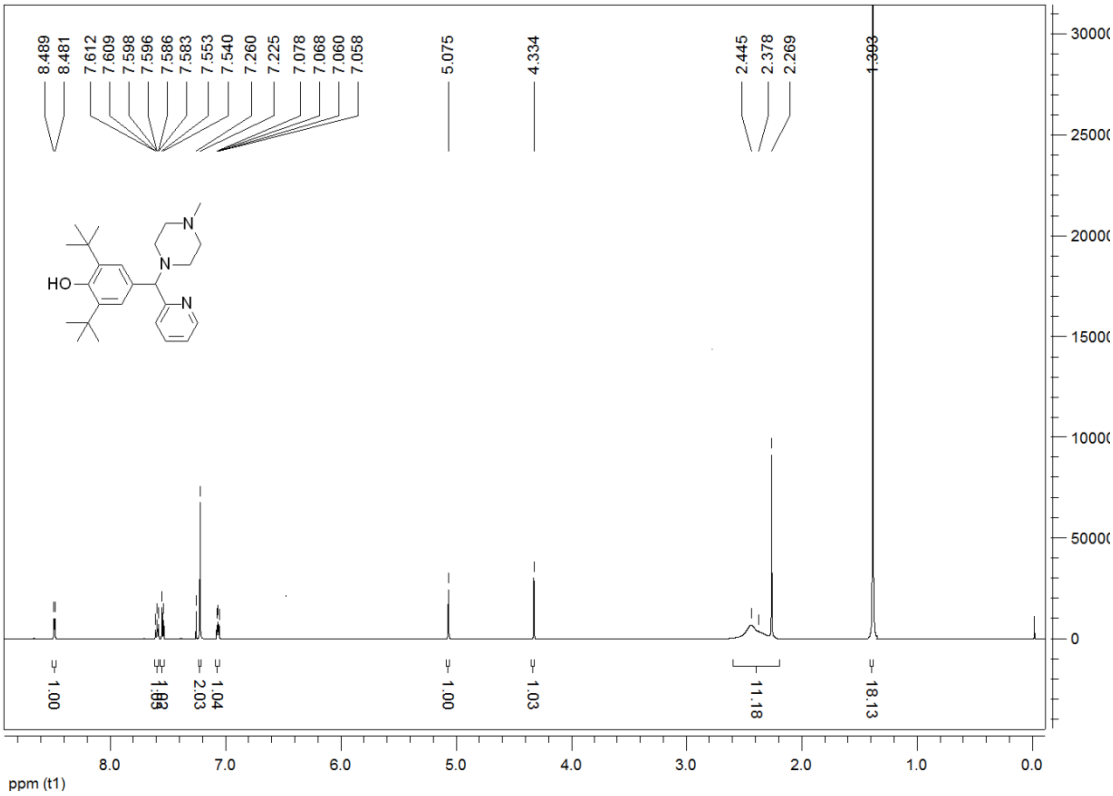

Fig.3 ^{1}H NMR of compound **CH-H-2**

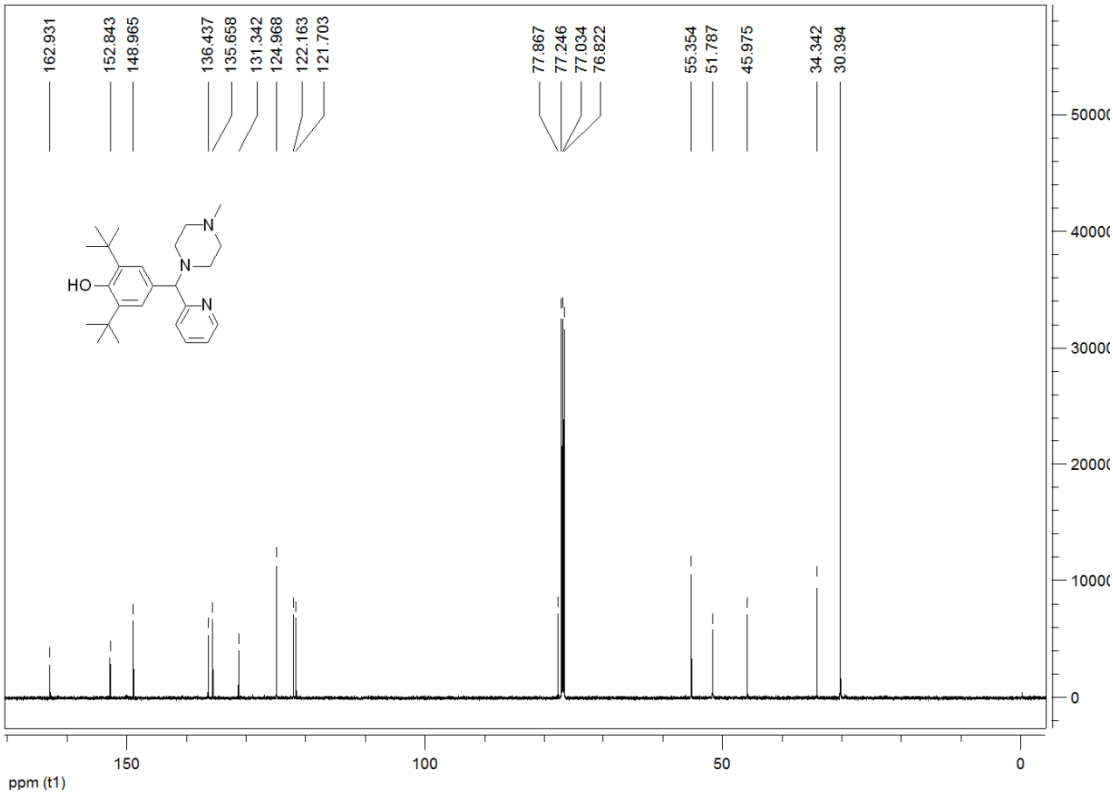

Fig.4 ^{13}C NMR of compound **CH-H-2**

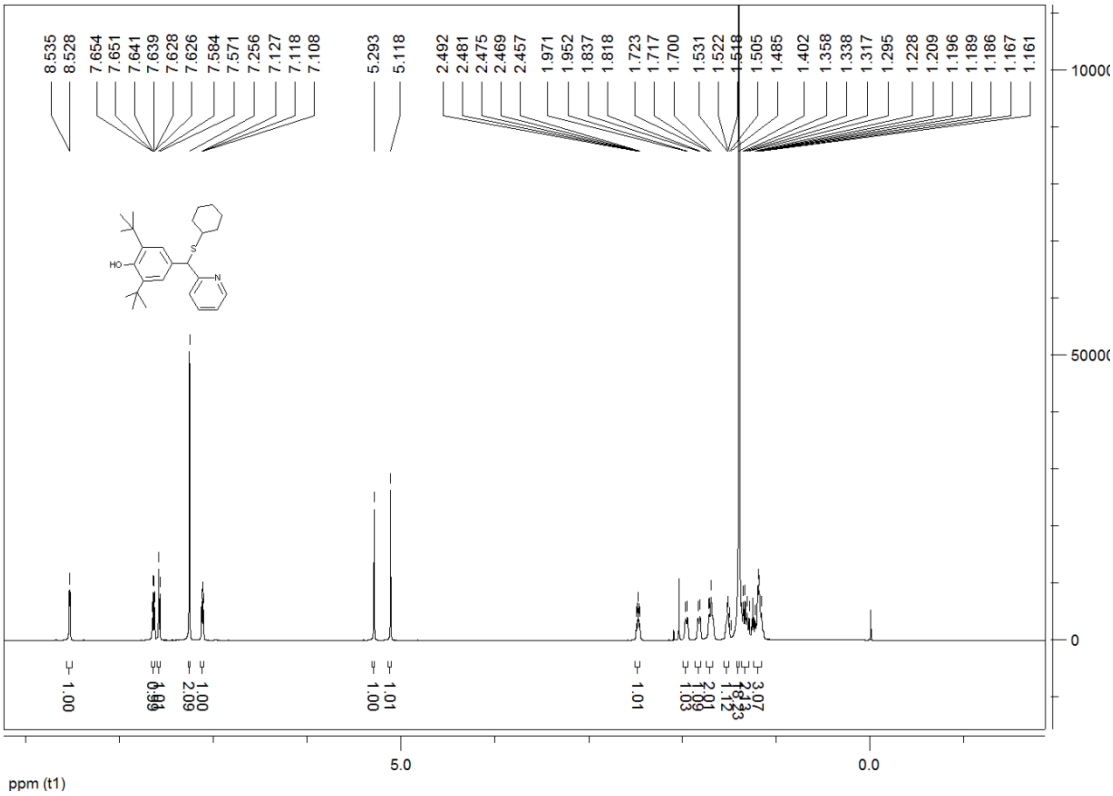

Fig.5 ^{1}H NMR of compound **CH-H-3**

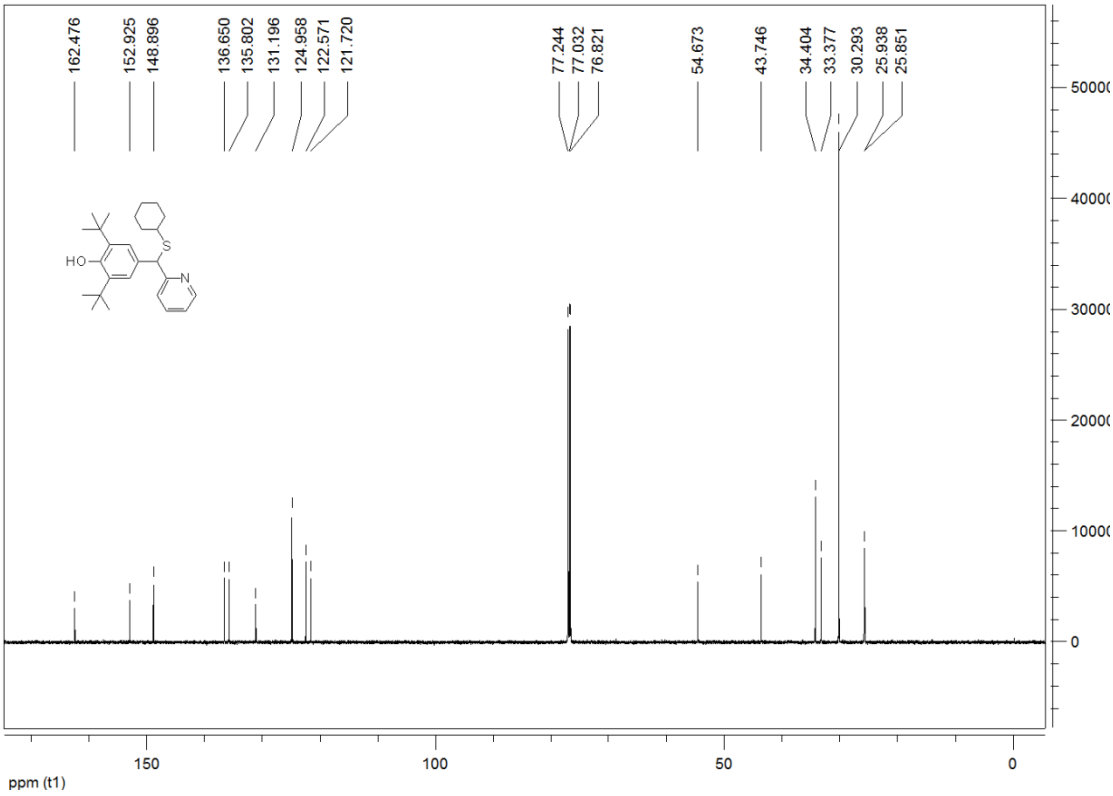

Fig.6 ^{13}C NMR of compound **CH-H-3**

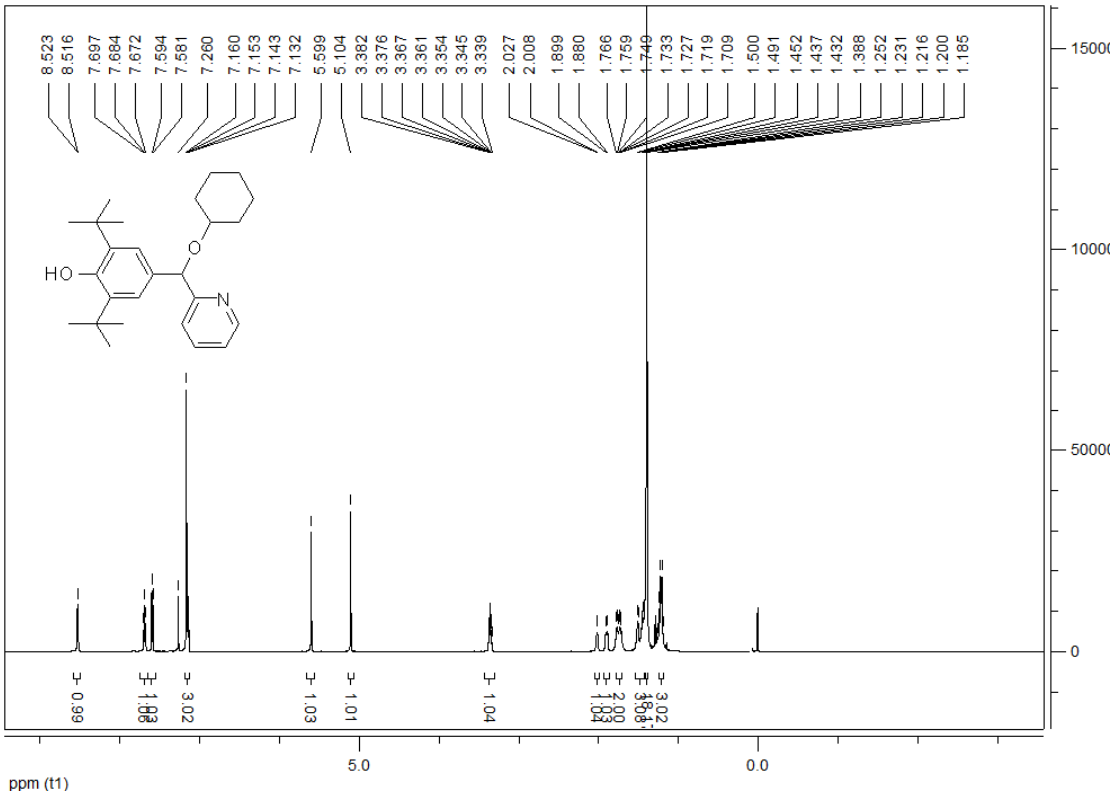

Fig.7 ^{1}H NMR of compound **CH-H-4**

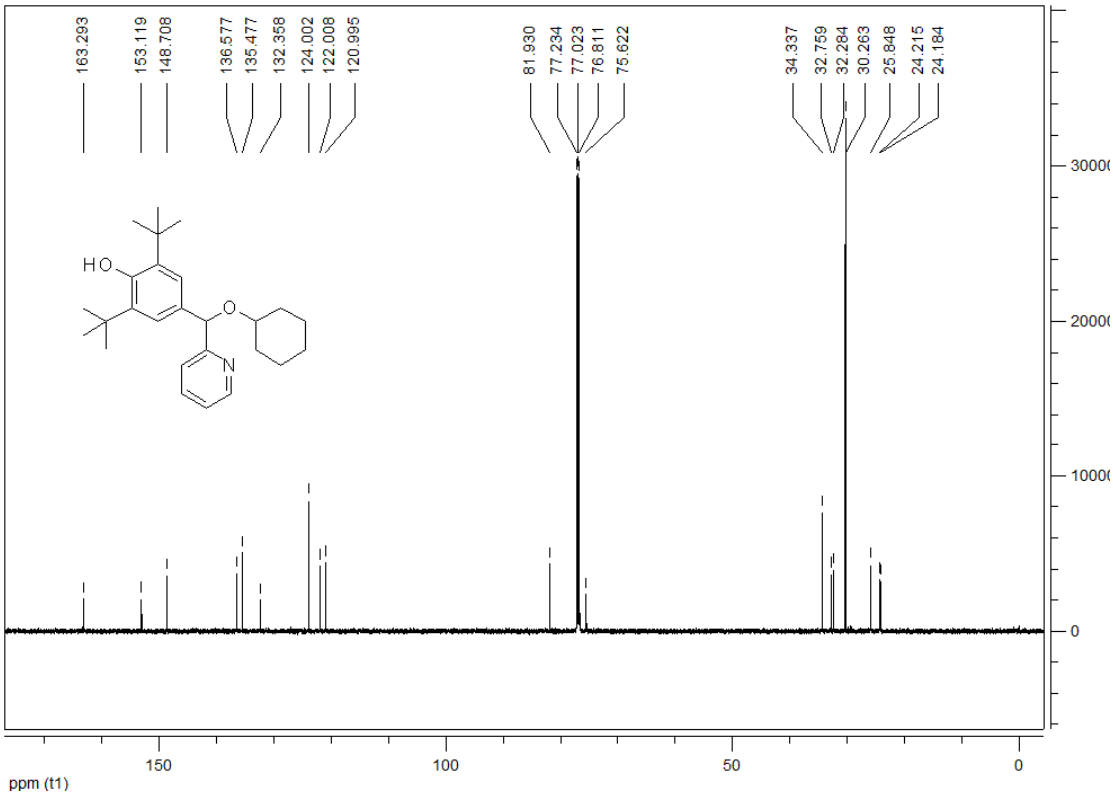

Fig.8 ^{13}C NMR of compound **CH-H-4**

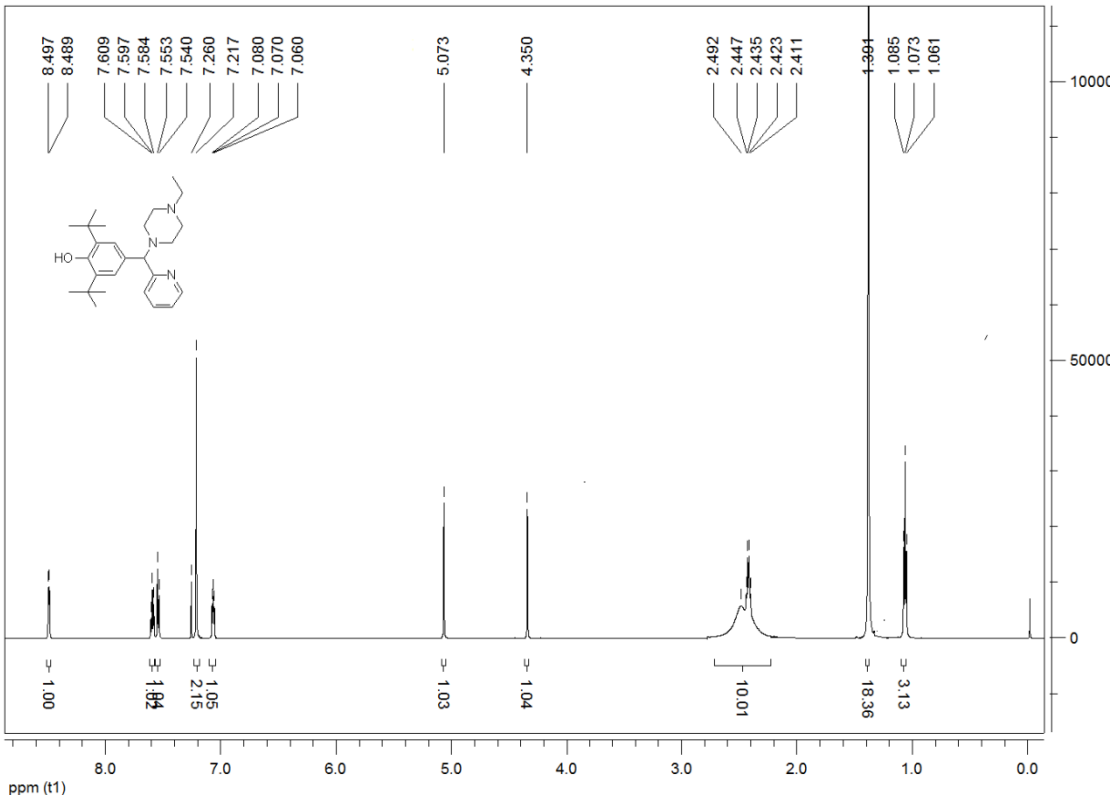

Fig.9 ^{1}H NMR of compound **CH-H-5**

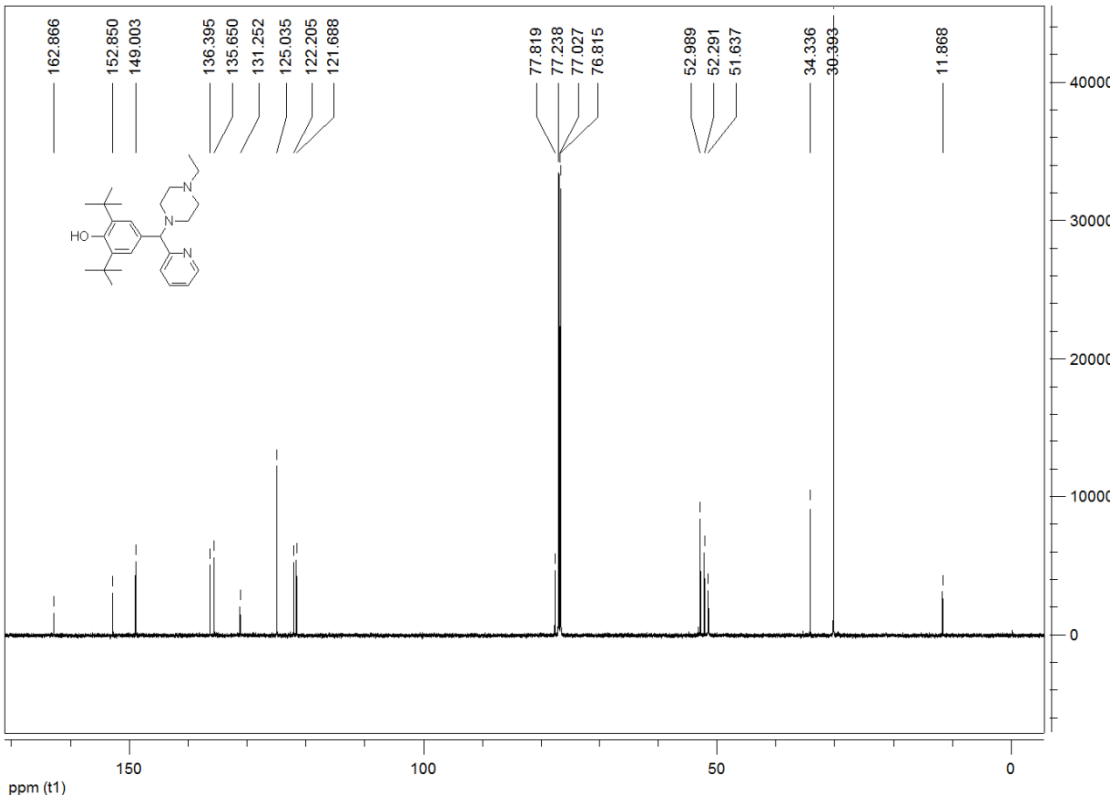

Fig.10 ^{13}C NMR of compound **CH-H-5**

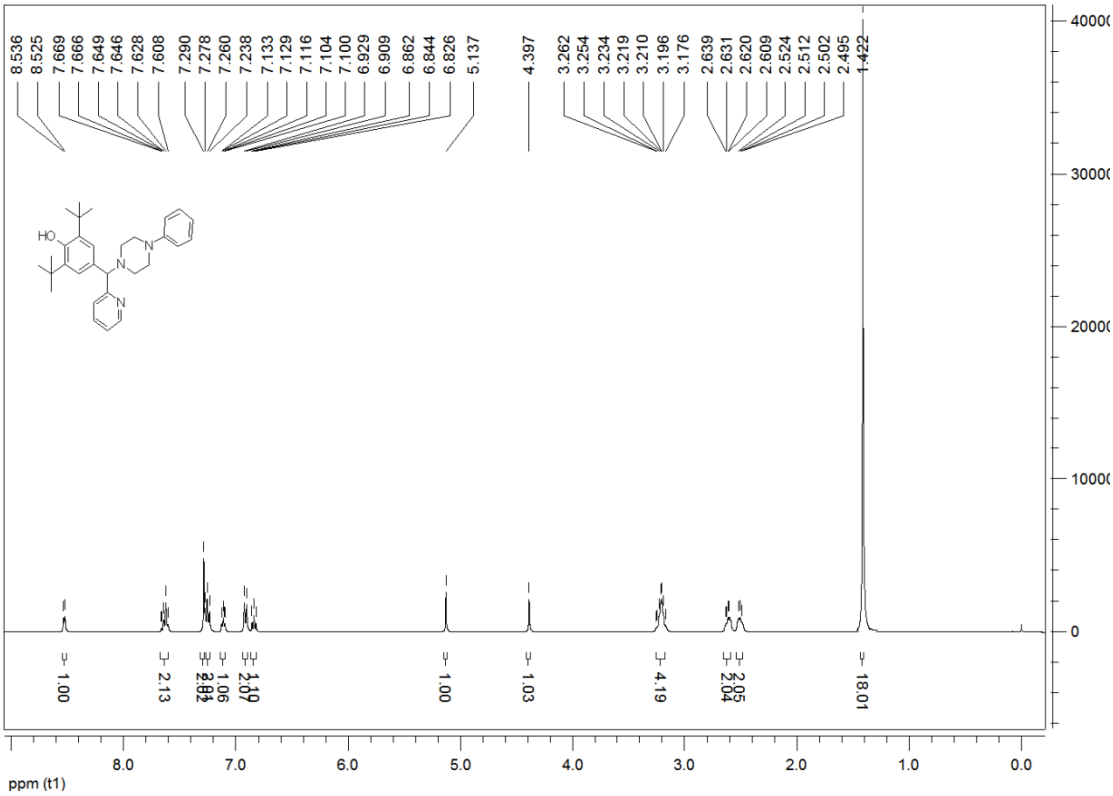

Fig.11 ^{1}H NMR of compound **CH-H-6**

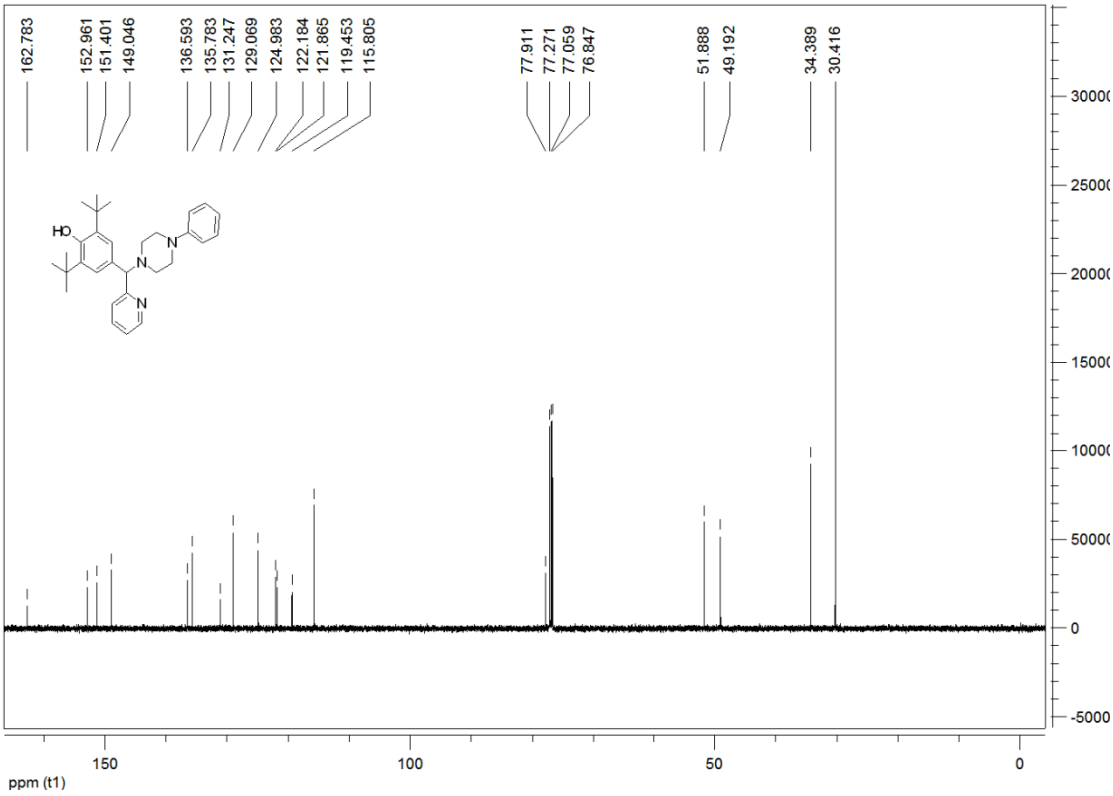

Fig.12 ^{13}C NMR of compound **CH-H-6**

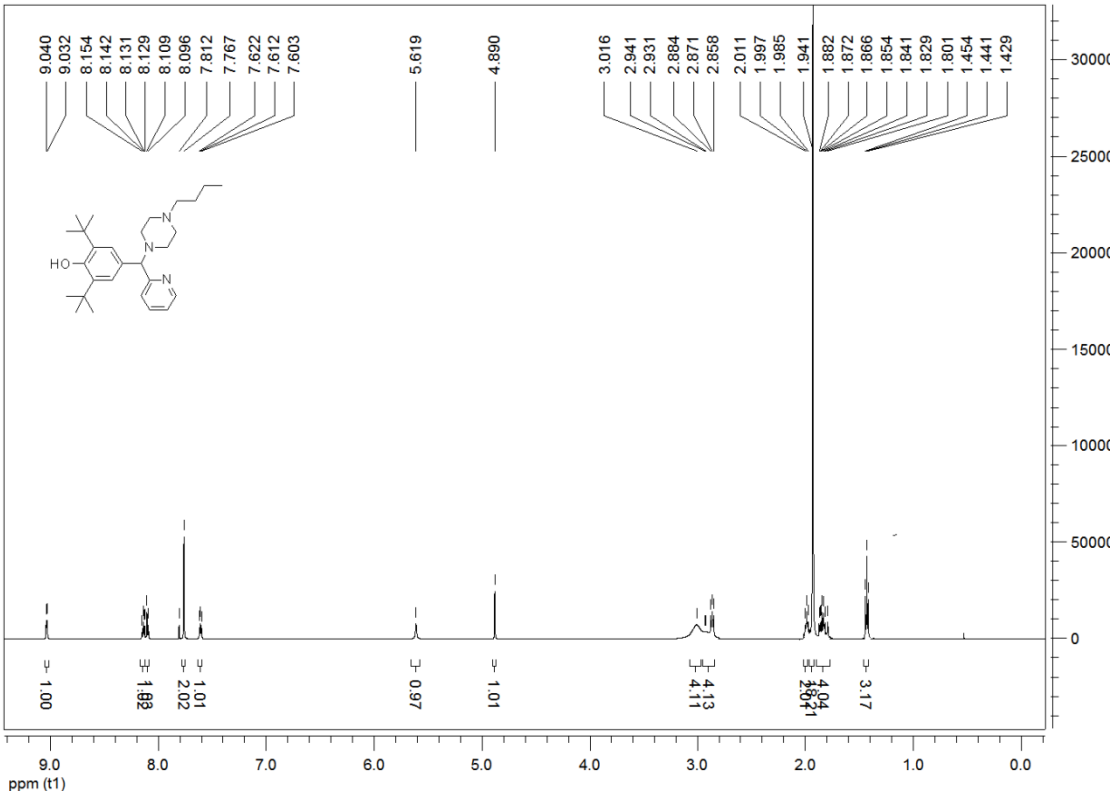

Fig.13 ^{1}H NMR of compound **CH-H-7**

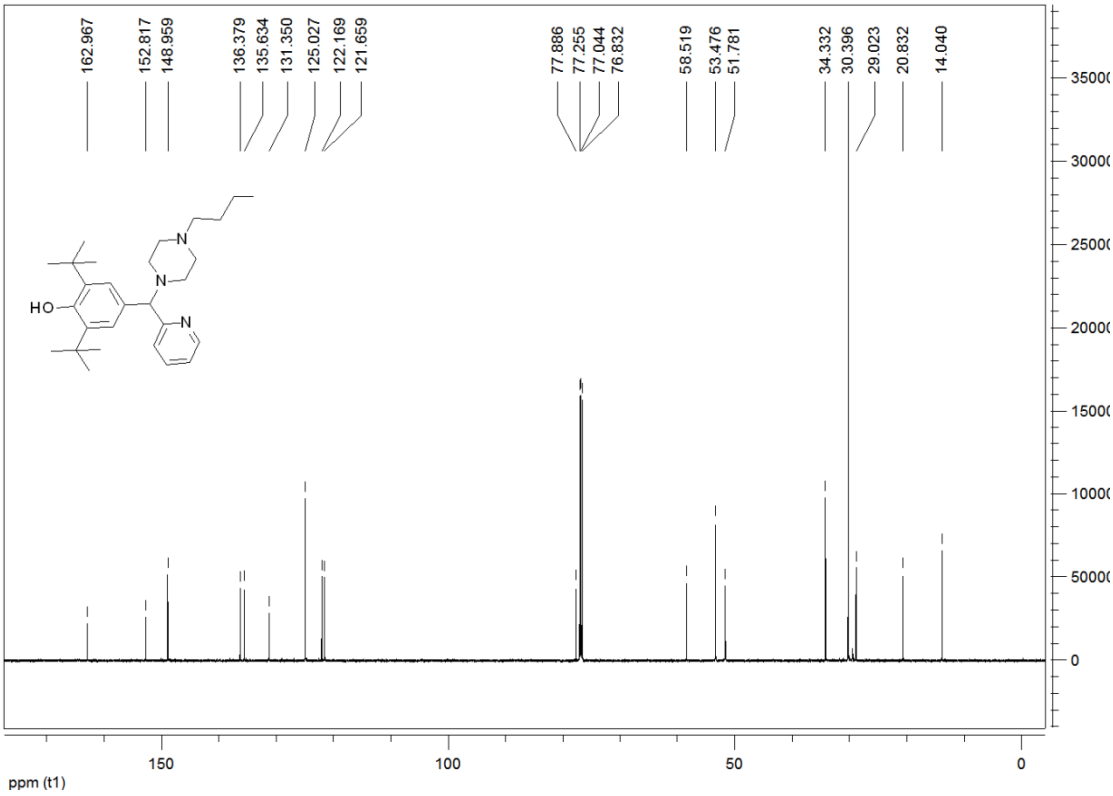

Fig.14 ^{13}C NMR of compound **CH-H-7**

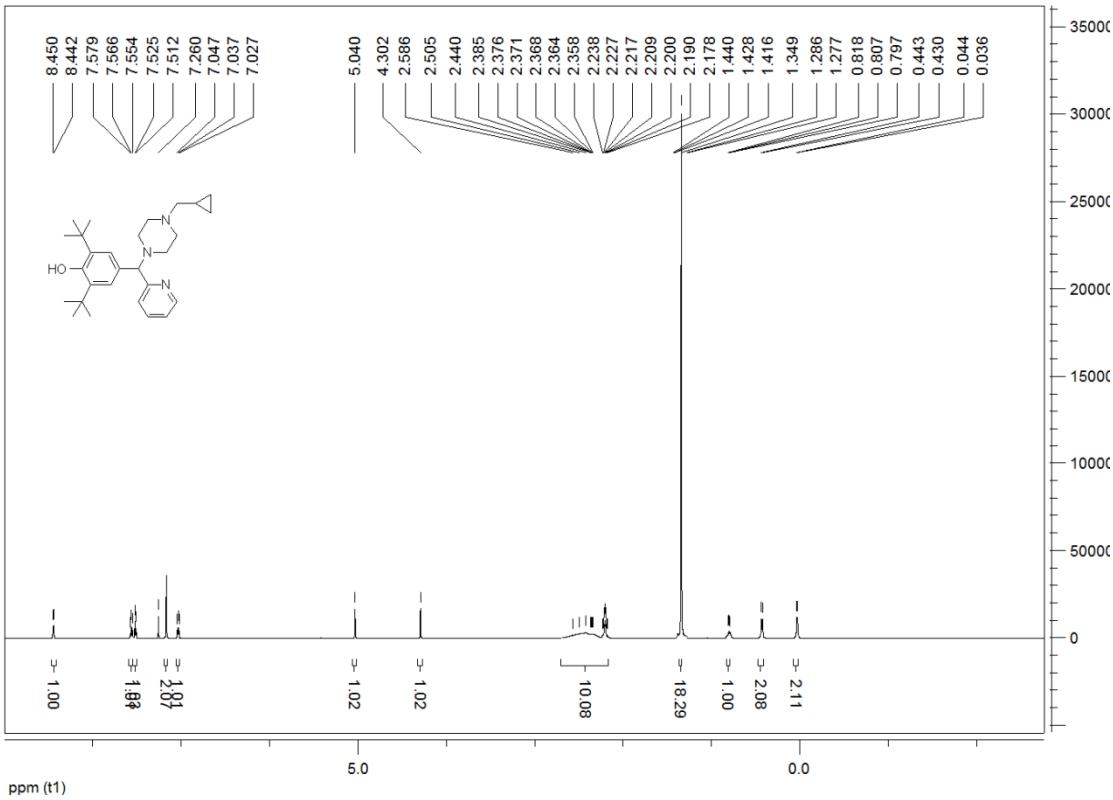

Fig.15 ^{1}H NMR of compound **CH-H-8**

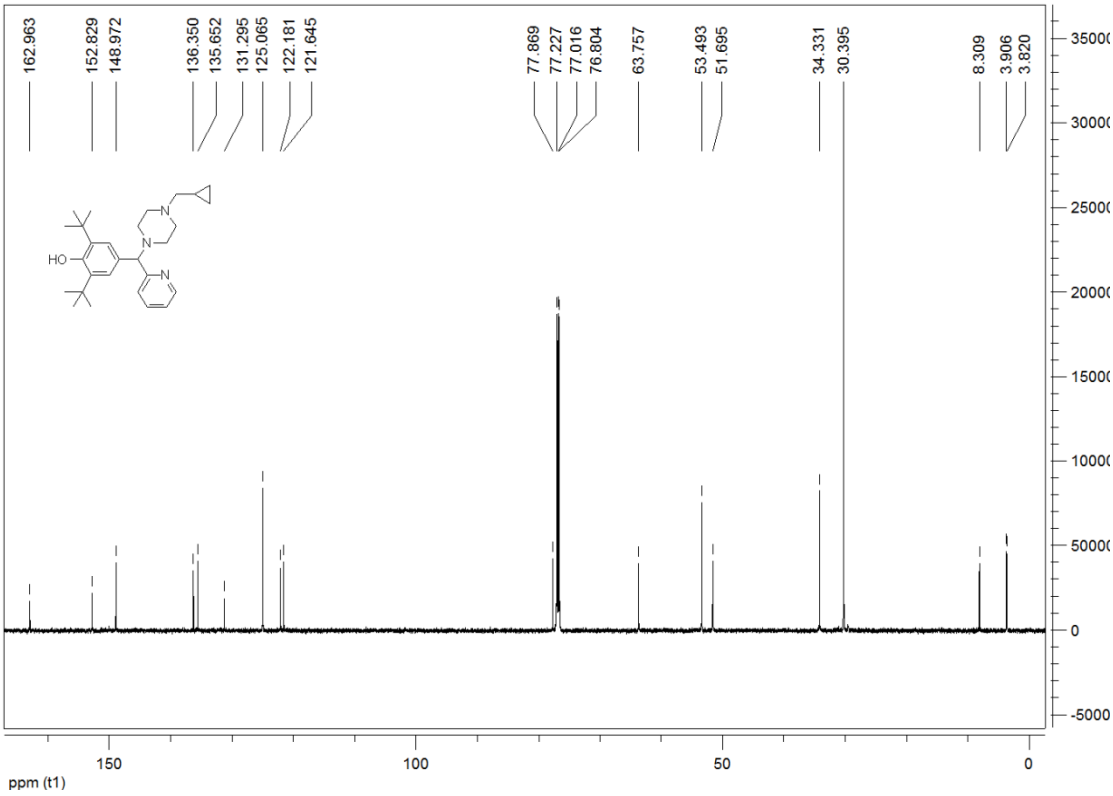

Fig.16 ^{13}C NMR of compound **CH-H-8**

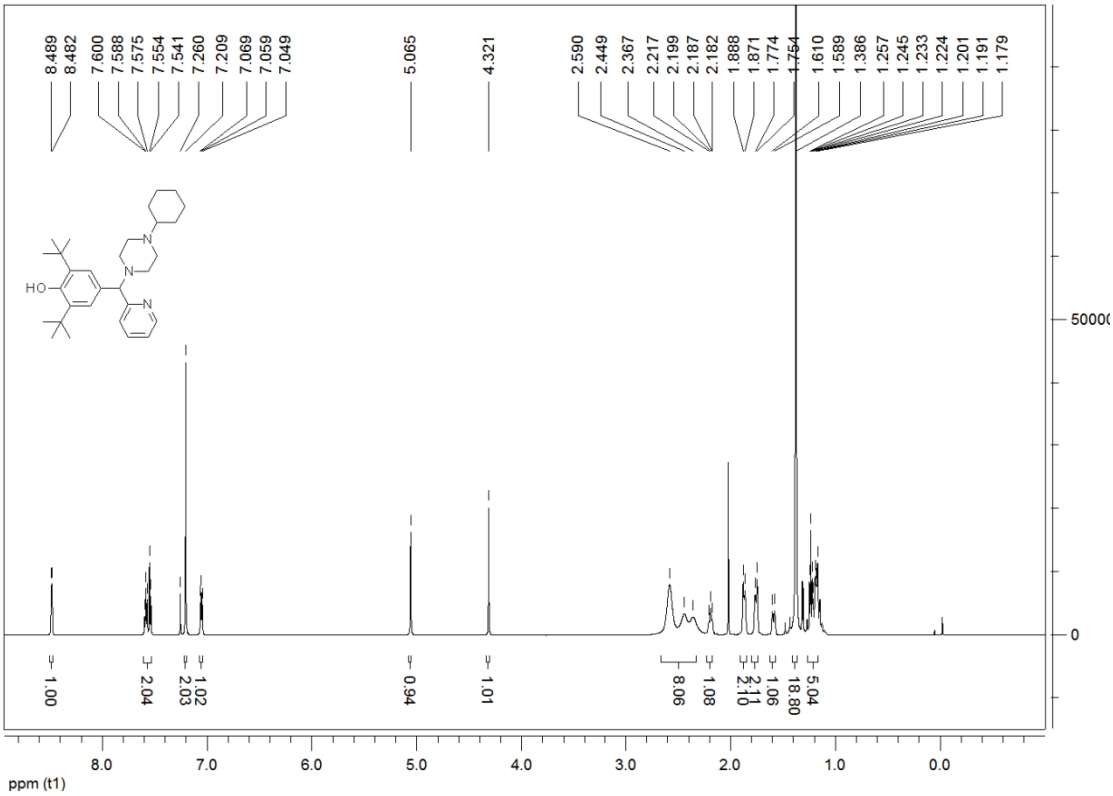

Fig.17 ^{1}H NMR of compound **CH-H-9**

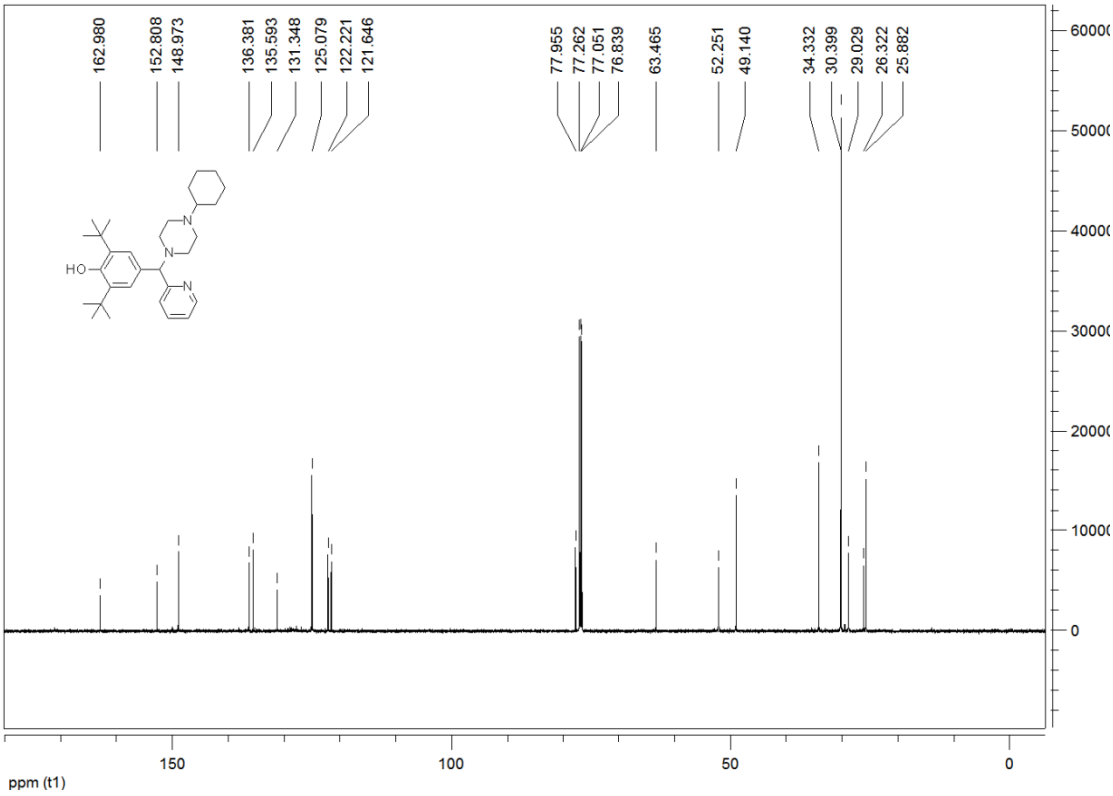

Fig.18 ^{13}C NMR of compound **CH-H-9**

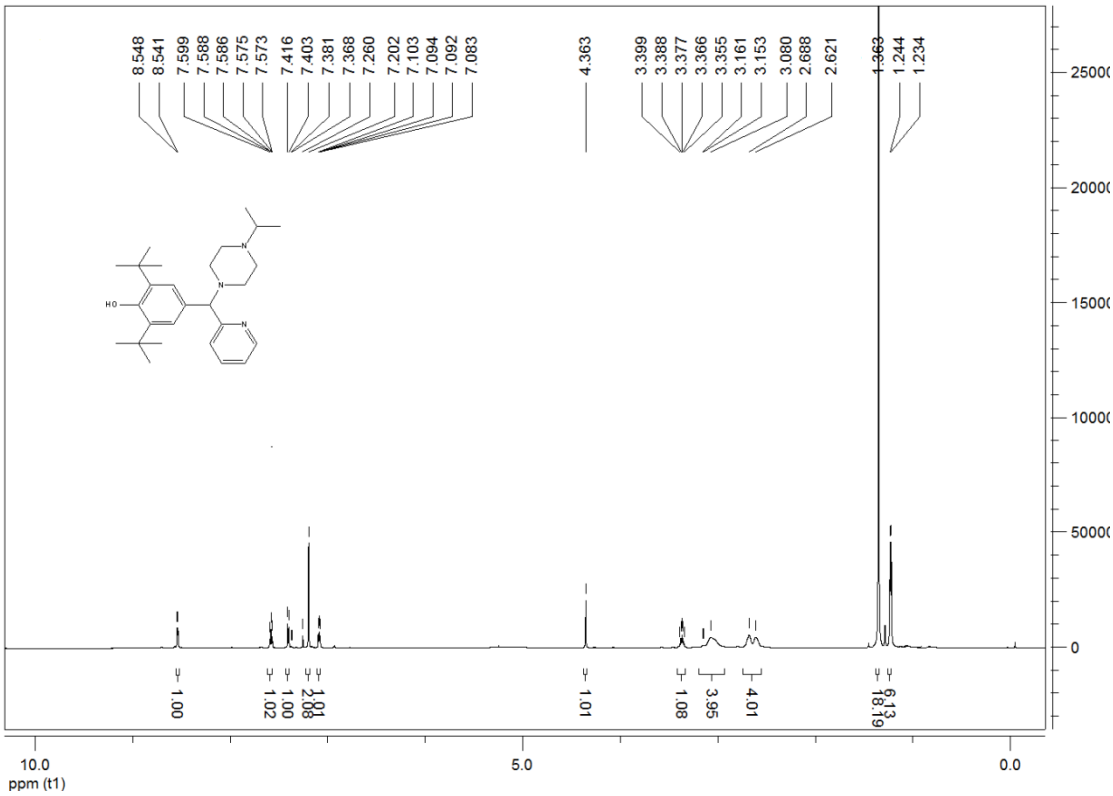

Fig.19 ^{1}H NMR of compound **CH-H-10**

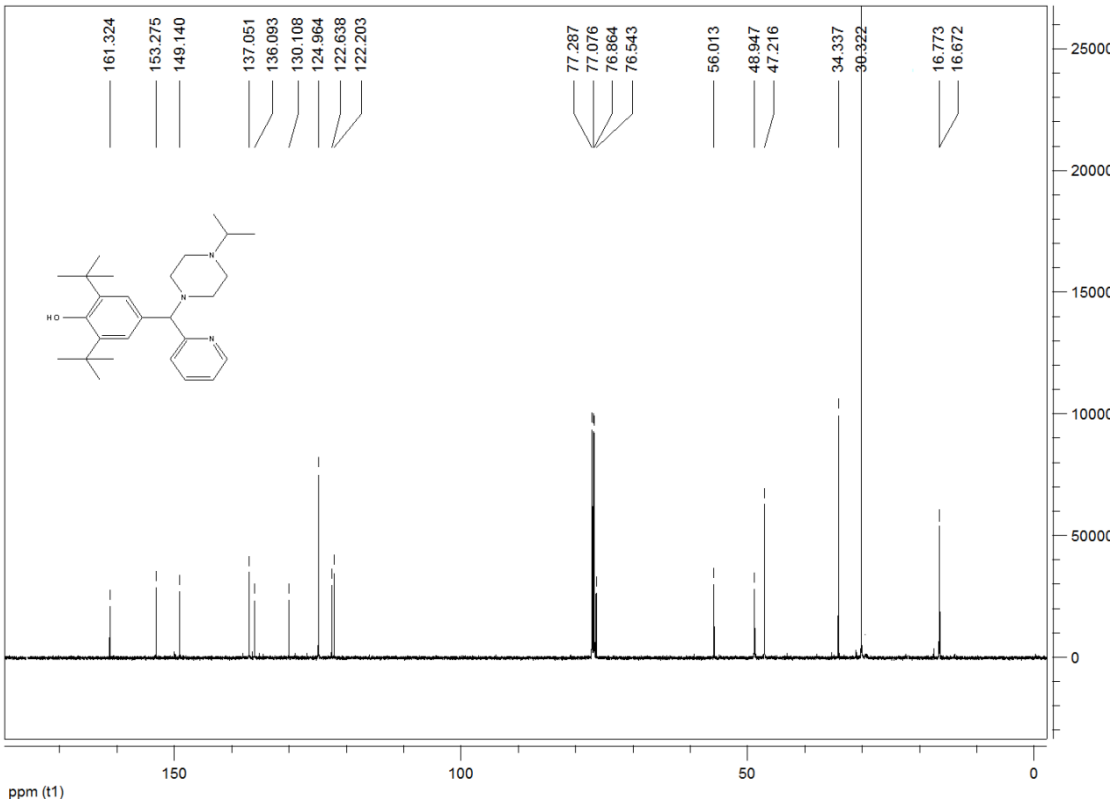

Fig.20 ^{13}C NMR of compound **CH-H-10**

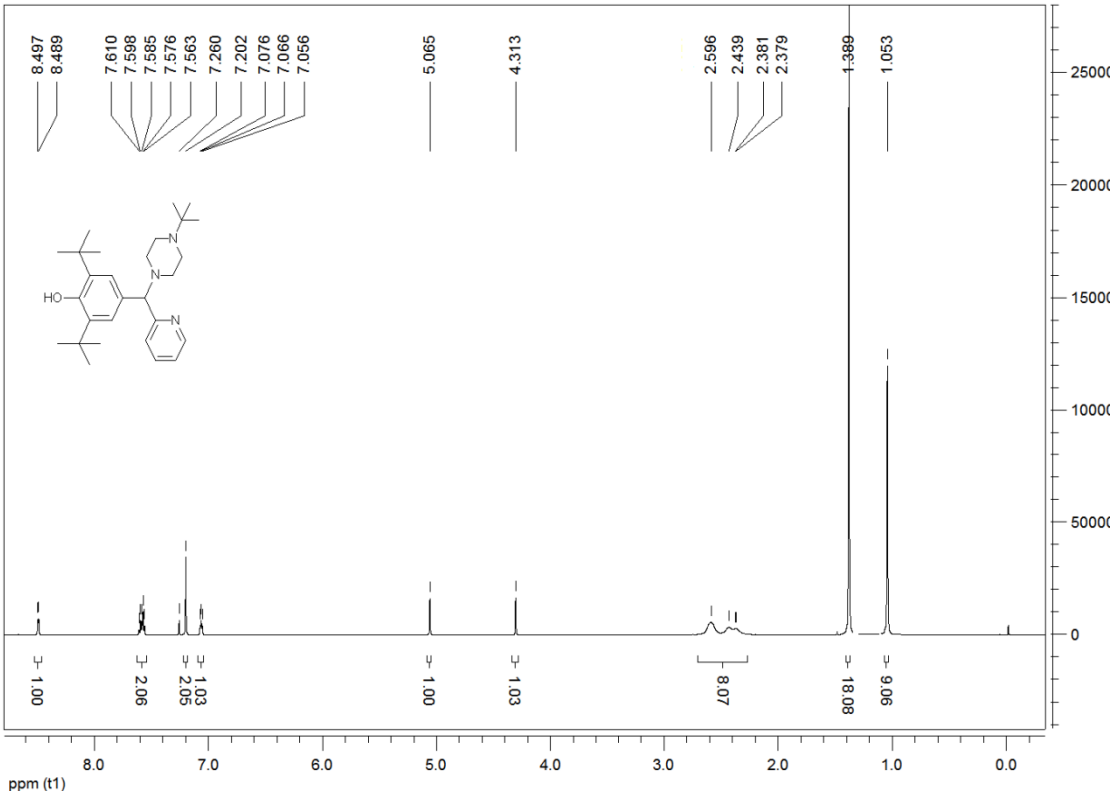

Fig.21 ^{1}H NMR of compound **CH-H-11**

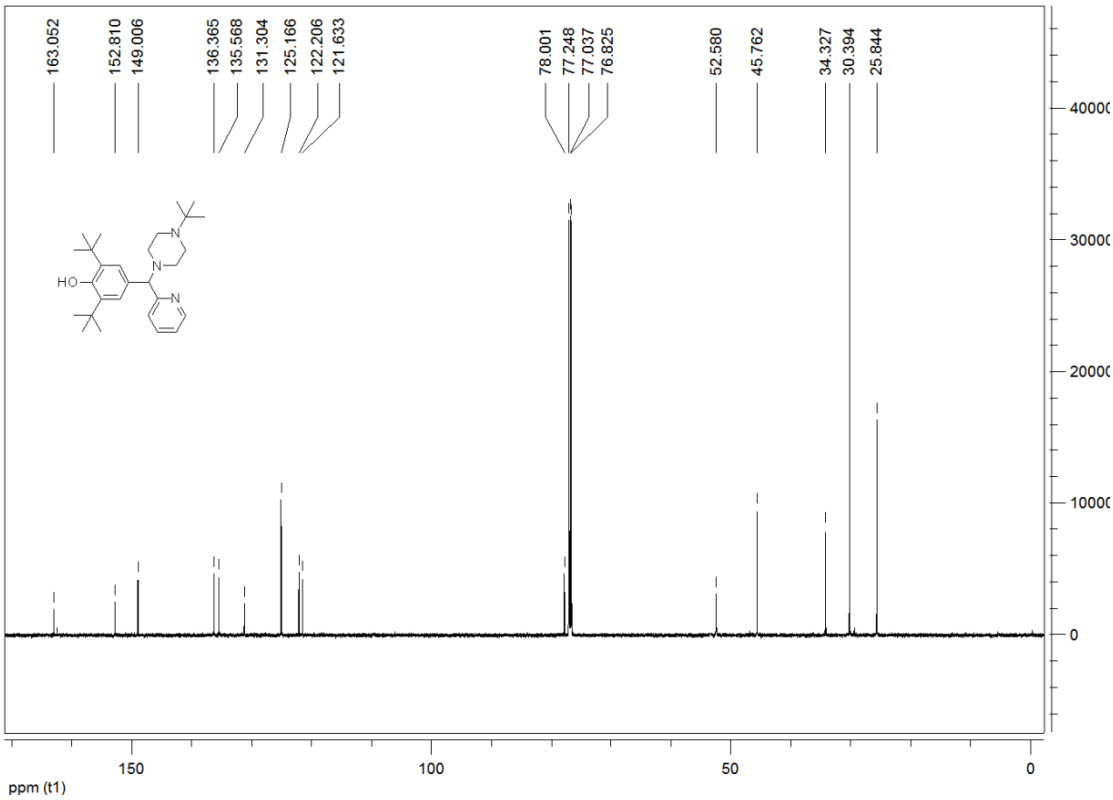

Fig.22 ^{13}C NMR of compound **CH-H-11**

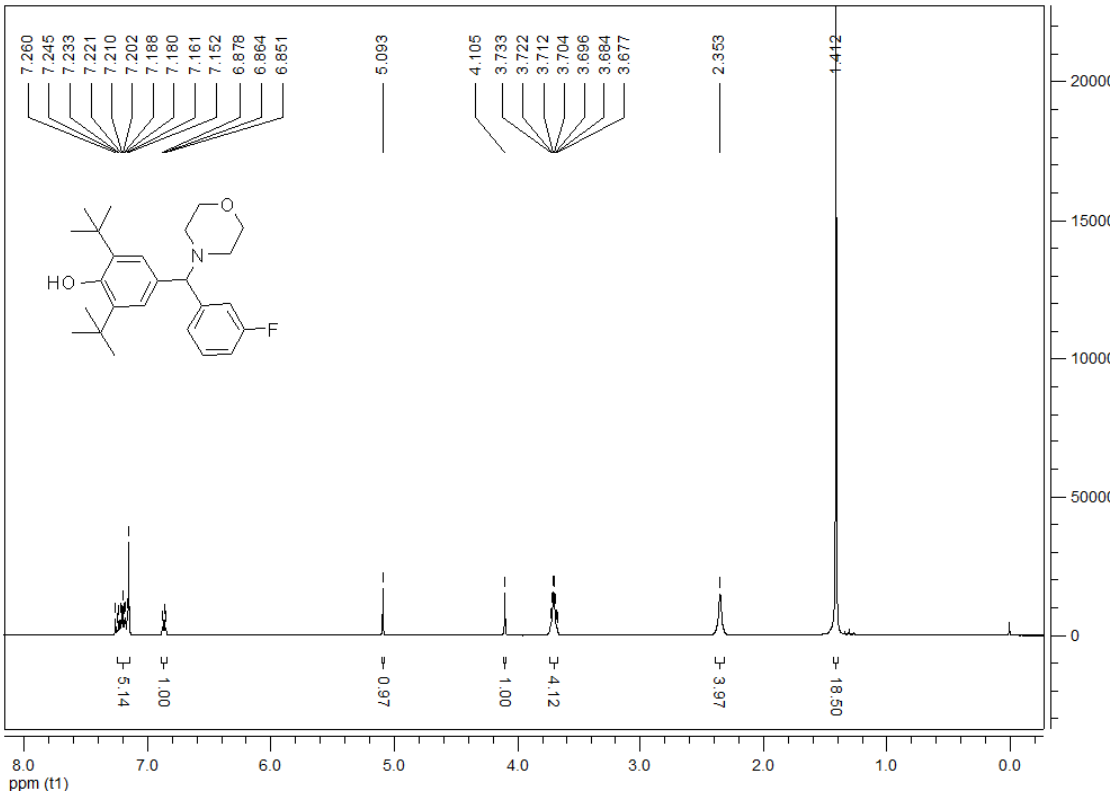

Fig.23 ^{1}H NMR of compound **CH-H-12**

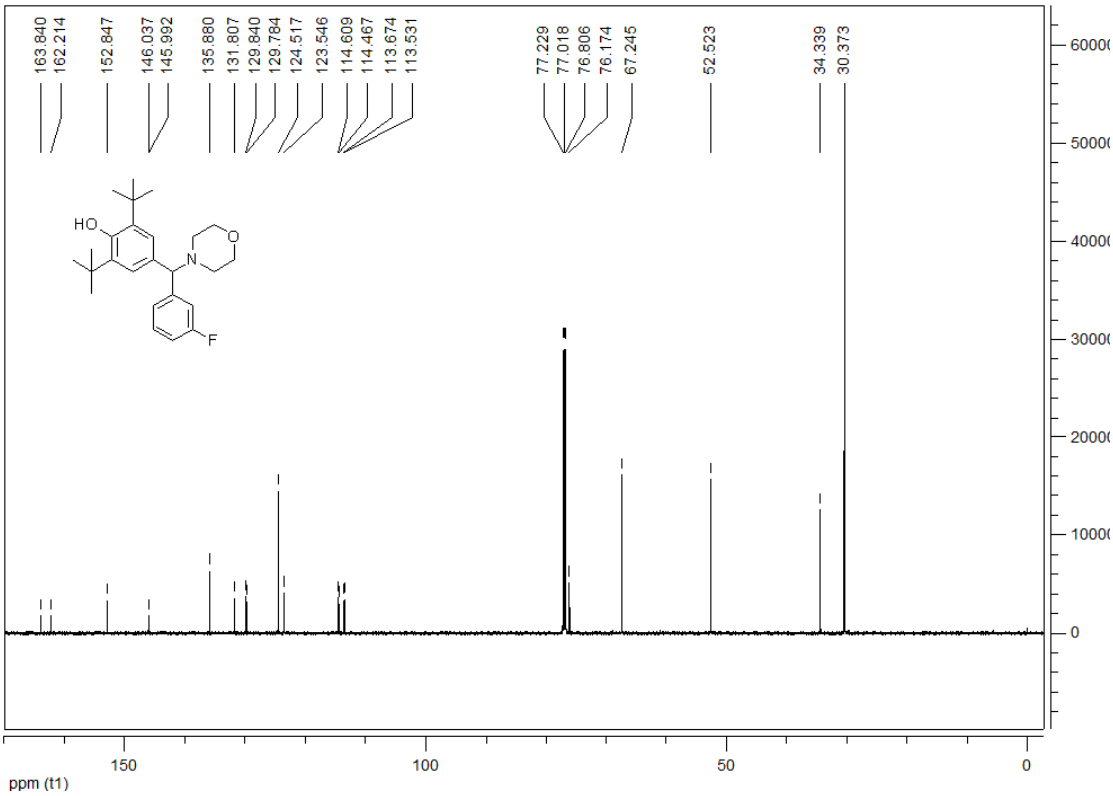

Fig.24 ^{13}C NMR of compound **CH-H-12**

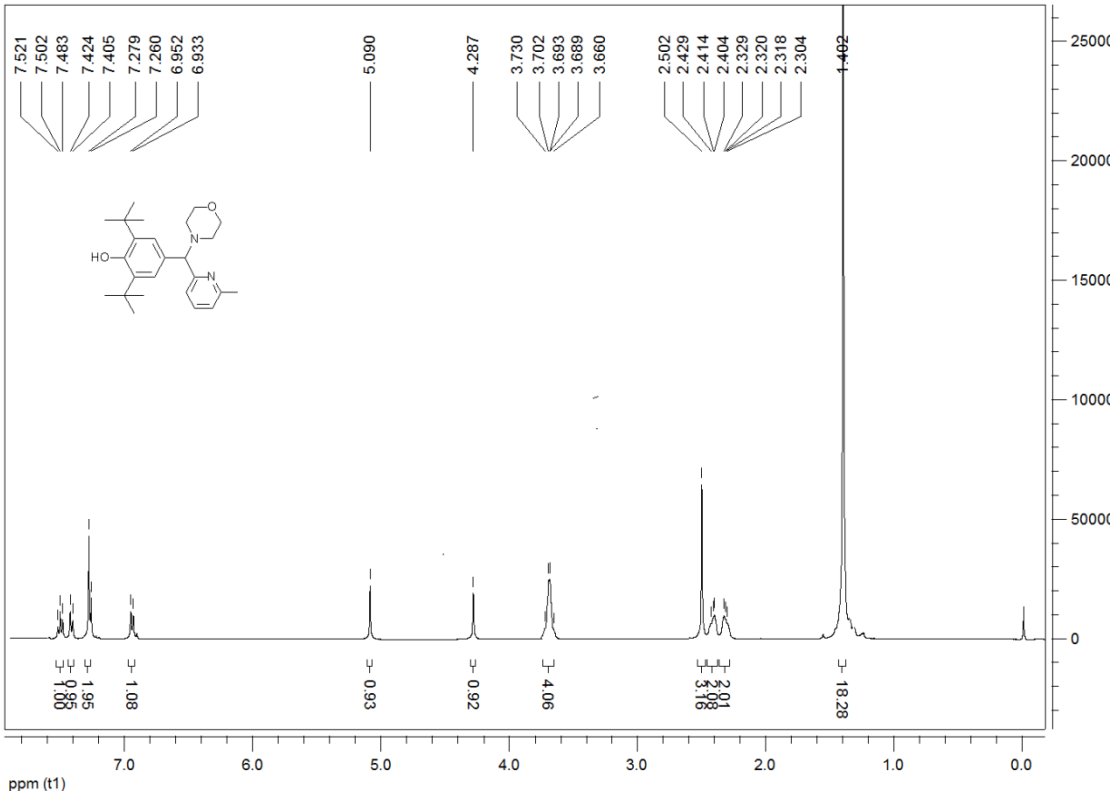

Fig.25 ^{1}H NMR of compound **CH-H-13**

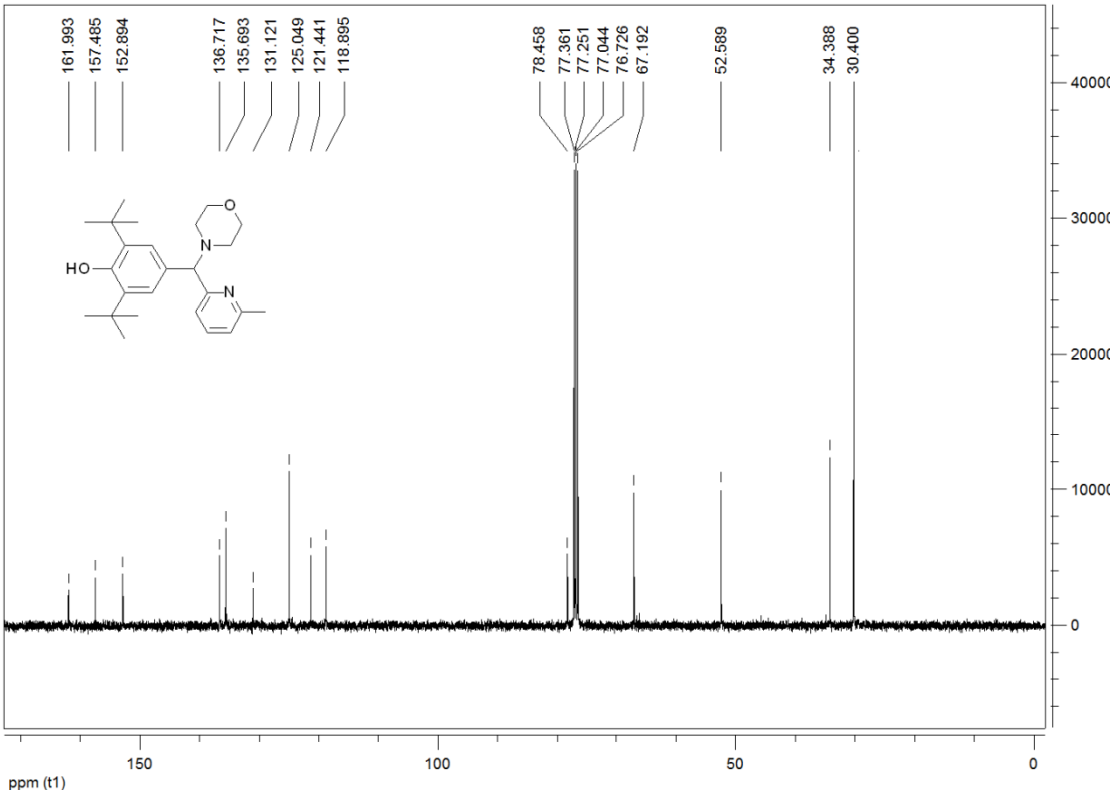

Fig.26 ^{13}C NMR of compound **CH-H-13**

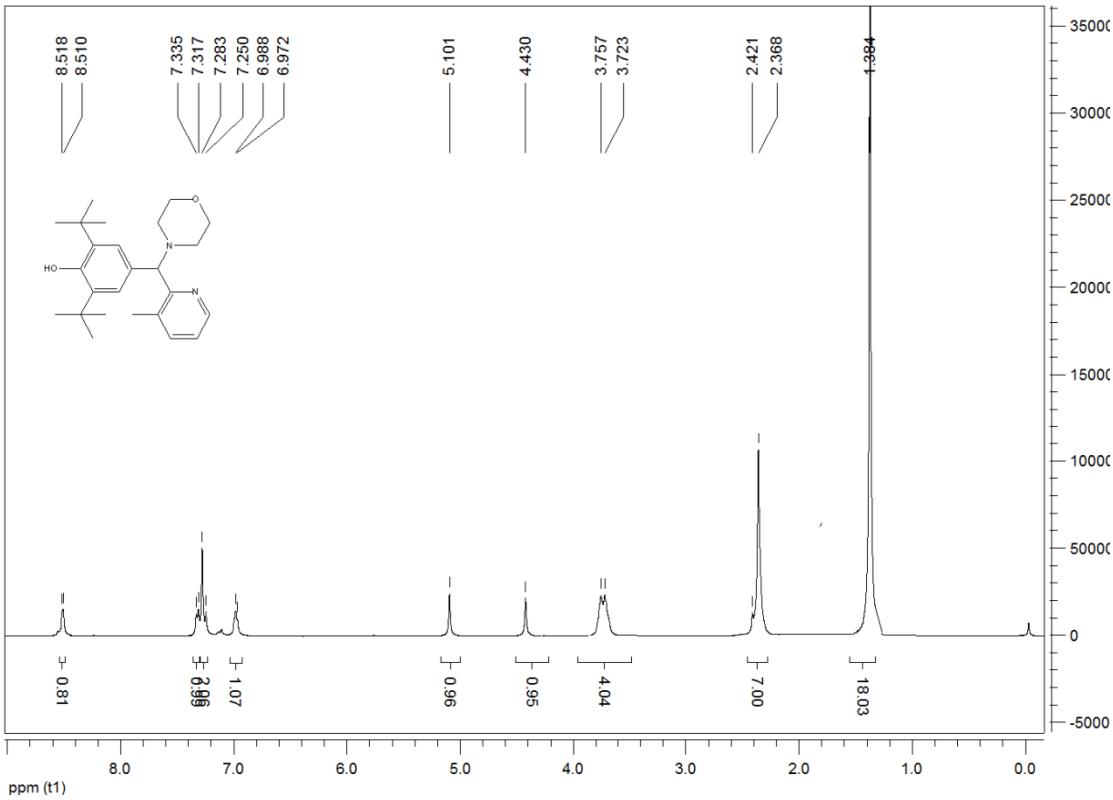

Fig.27 ^{1}H NMR of compound **CH-H-14**

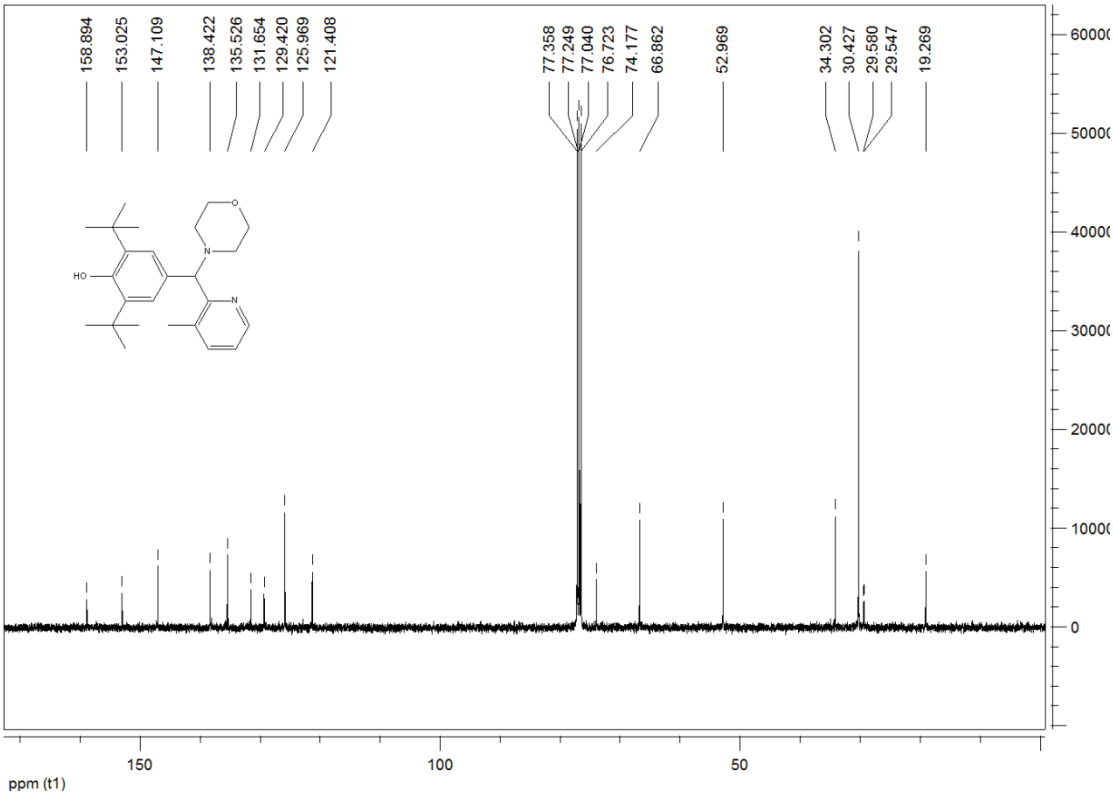

Fig.28 ^{13}C NMR of compound **CH-H-14**

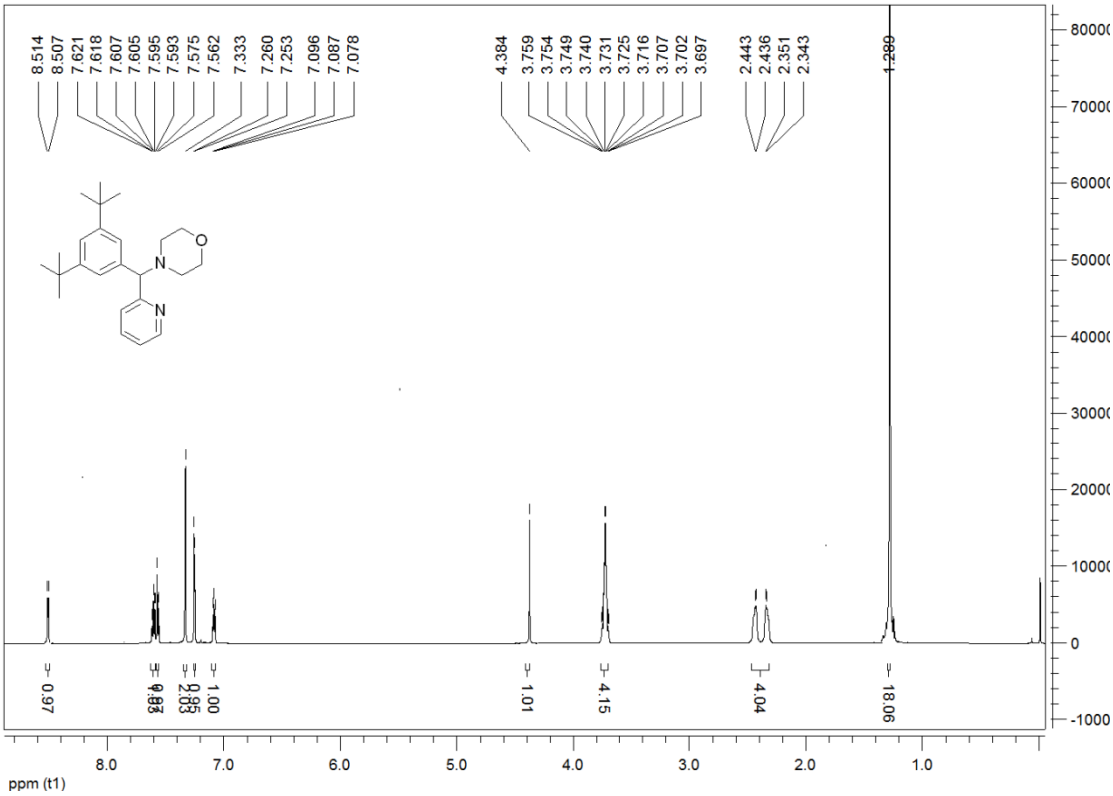

Fig.29 ^{1}H NMR of compound **CH-H-15**

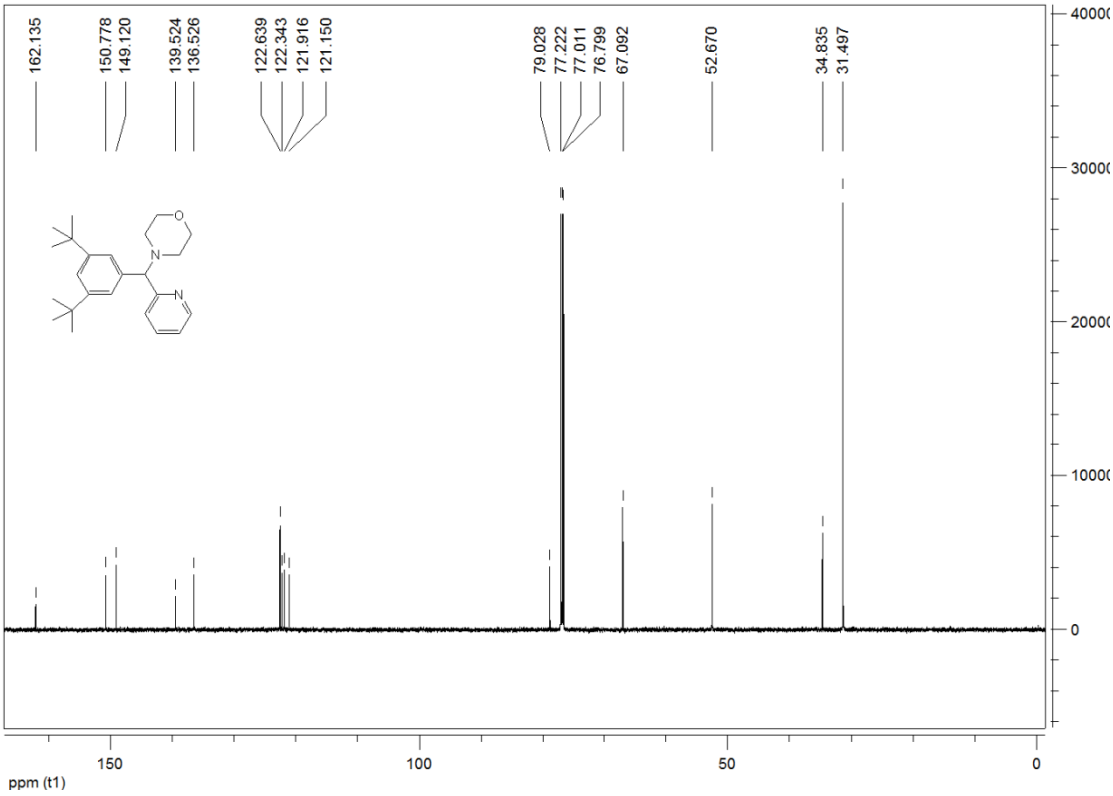

Fig.30 ^{13}C NMR of compound **CH-H-15**

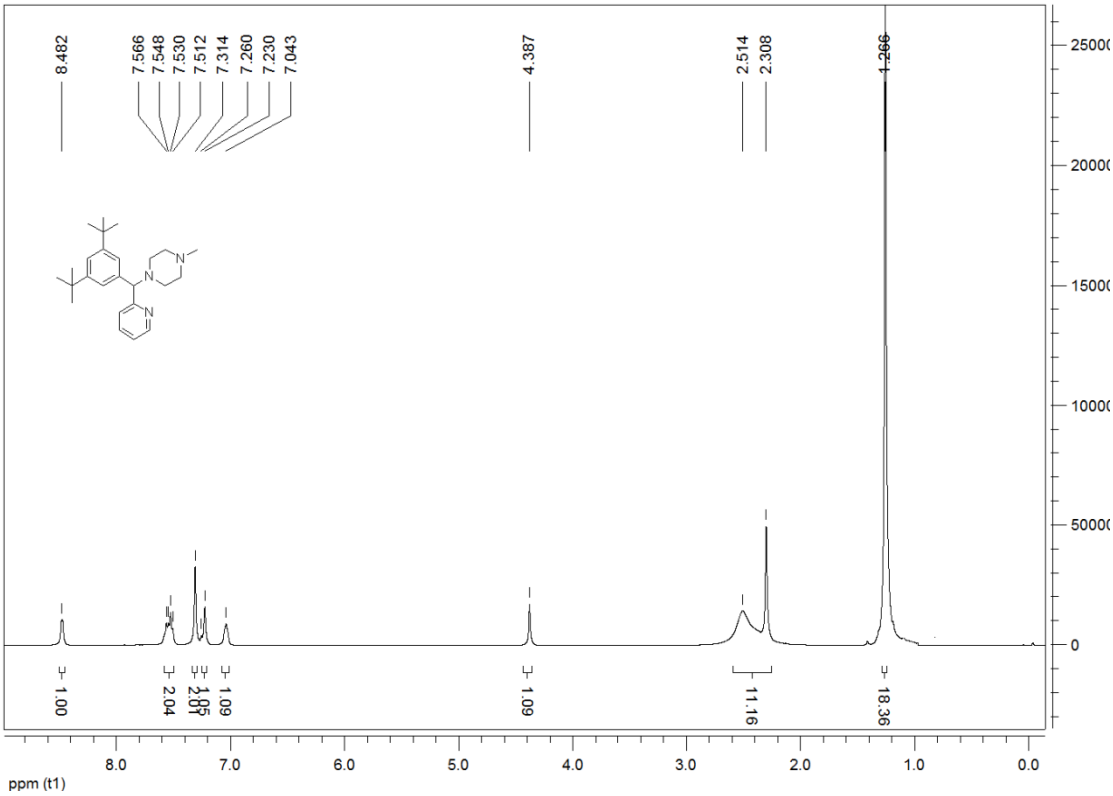

Fig.31 ^{1}H NMR of compound **CH-H-16**

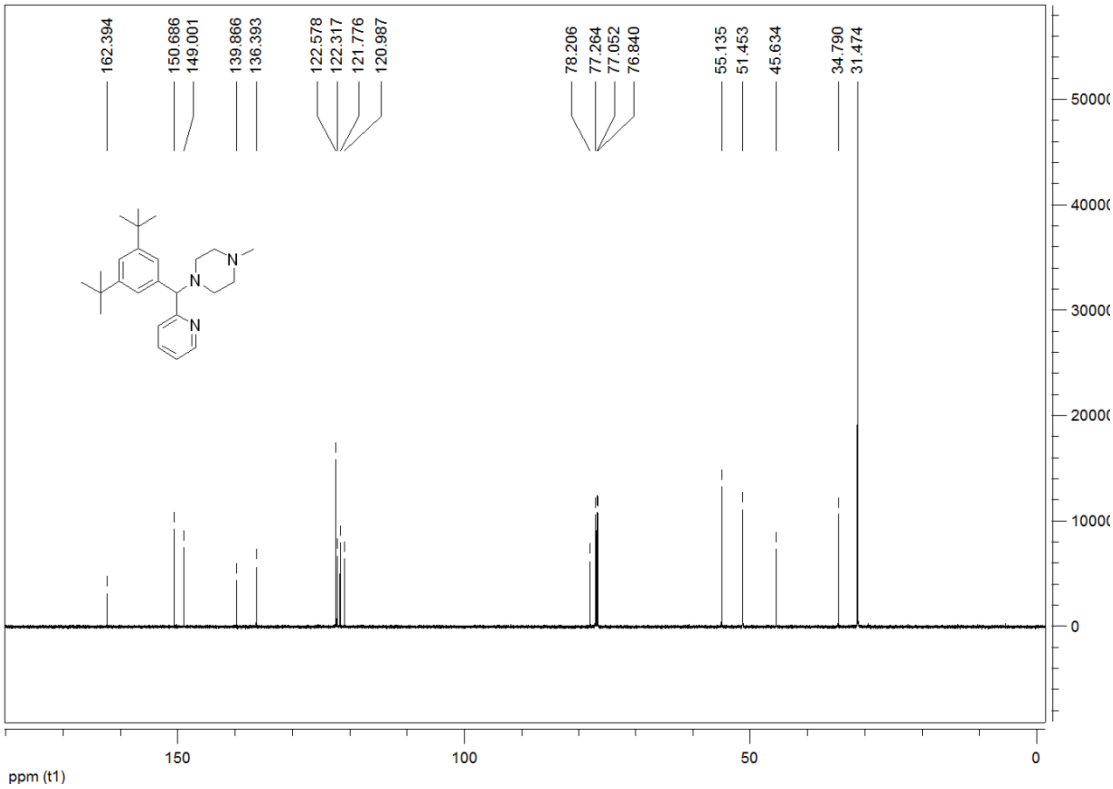

Fig.32 ^{13}C NMR of compound **CH-H-16**

Table 1. Structures and biochemical IC_{50} (μmol/L) data for DC_H31 and its analogues.

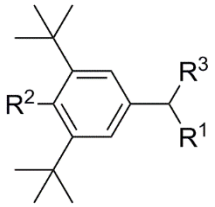

Compounds.	R^1	R^2	R^3	Biochemical IC_{50}(μmol/L) IDH1-R132H	IDH1-R132C	WT IDH1
CH-H-1	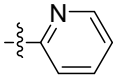	**OH**	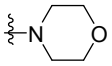	0.41	2.7	43.7
CH-H-2	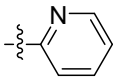	**OH**	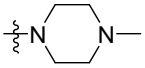	3.0	4.9	~50
CH-H-3	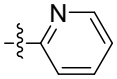	**OH**	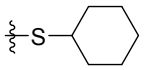	>50	>50	>50
CH-H-4	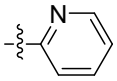	**OH**	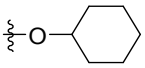	>50	>50	>50
CH-H-5	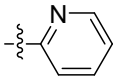	**OH**	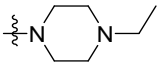	12	4.8	6.4
CH-H-6	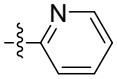	**OH**	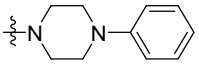	>50	>50	>50
CH-H-7	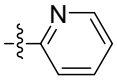	**OH**	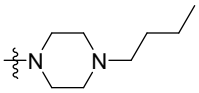	>50	9	12.79
CH-H-8	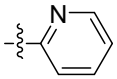	**OH**	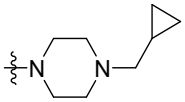	>50	18	31
CH-H-9	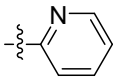	**OH**	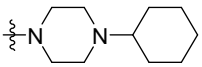	>50	>50	>50
CH-H-10	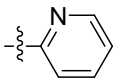	**OH**	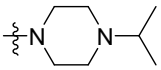	4.76	7	3
CH-H-11	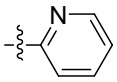	**OH**	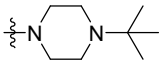	>50	9	8.5

CH-H-12	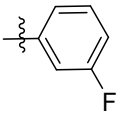	**OH**	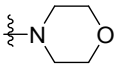	>50	>50	>50
CH-H-13	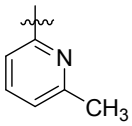	**OH**	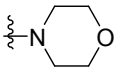	>50	>50	>50
CH-H-14	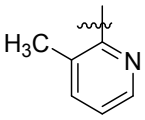	**OH**	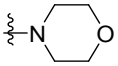	20	4.7	0.8
CH-H-15	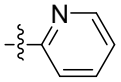	**H**	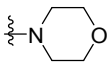	>50	>50	>50
CH-H-16	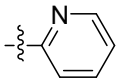	**H**	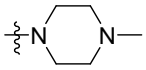	>50	>50	>50

Note: The IC_{50} values for IDH1-R132H and IDH1-R132C and WT IDH1 are the mean of three determinations performed as described method.

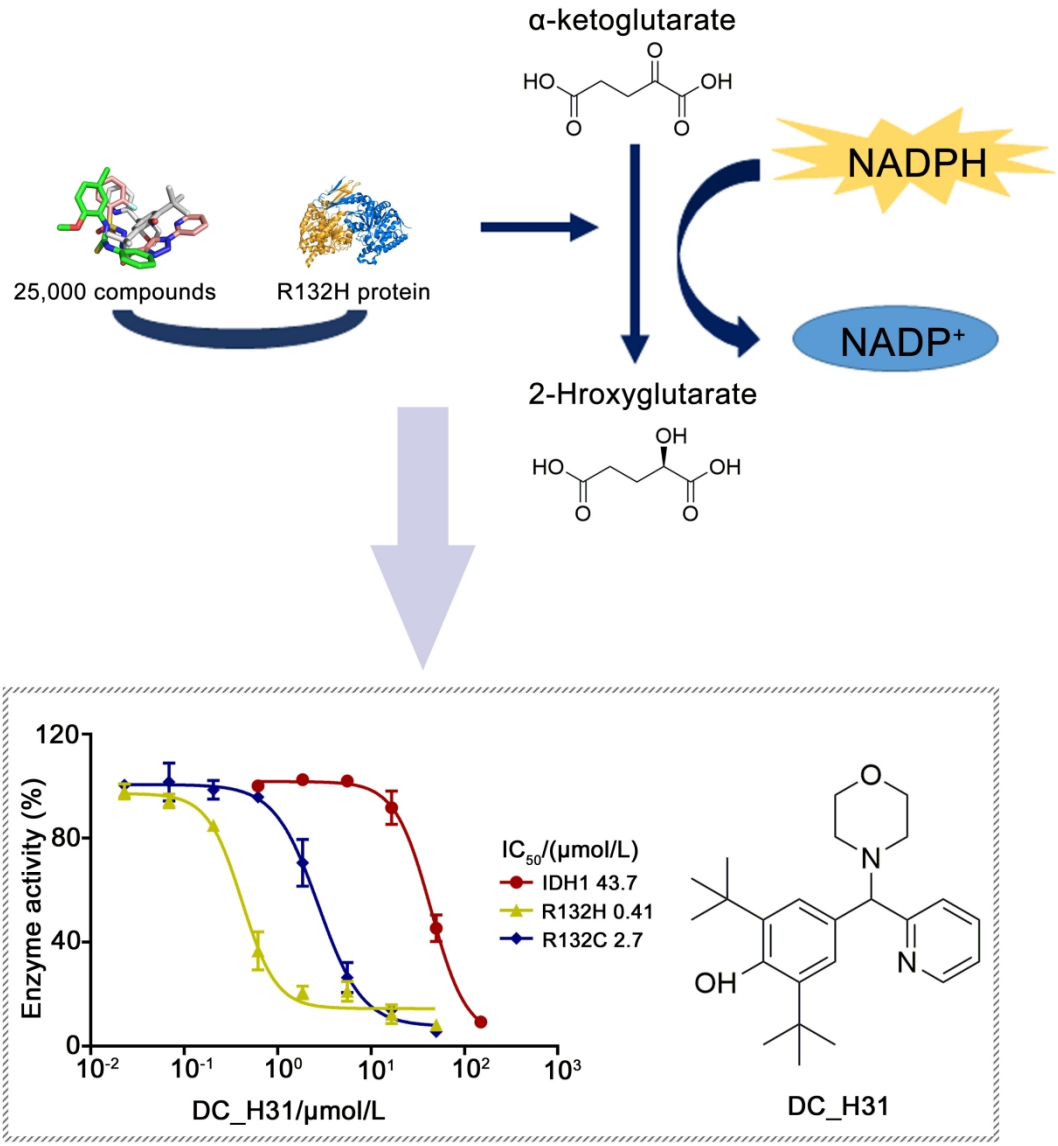
α-ketoglutarate
HO
O
O
OH
O
NADPH
25,000 compounds
R132H protein
NADP+
2-Hroxyglutarate
HO
OH
O
OH
O
120
80
40
0
Enzyme activity (%)
10-2
10-1
100
101
102
103
DC_H31/μmol/L
IC50/(μmol/L)
IDH1 43.7
R132H 0.41
R132C 2.7
O
N
N
OH
DC_H31

1

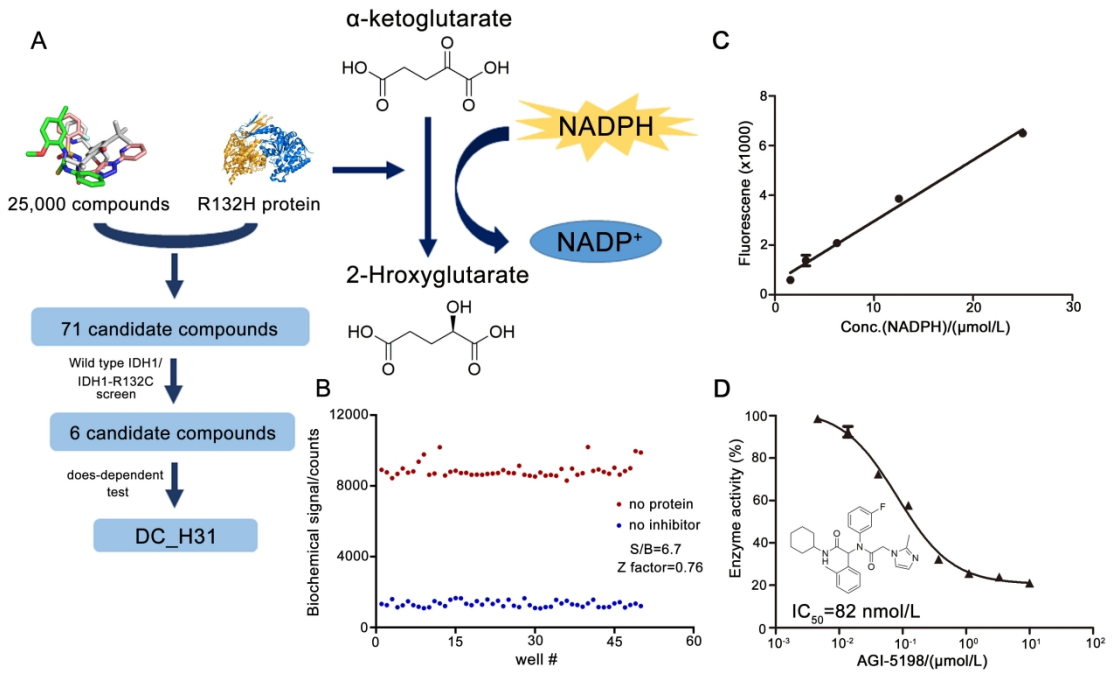
A
α-ketoglutarate
NADPH
NADP+
2-Hroxyglutarate
25,000 compounds
R132H protein
71 candidate compounds
Wild type IDH1/ IDH1-R132C screen
6 candidate compounds
does-dependent test
DC_H31
B
Biochemical signal/counts
no protein
no inhibitor
S/B=6.7
Z factor=0.76
well #
C
Fluorescene (x1000)
Conc.(NADPH)/(μmol/L)
D
Enzyme activity (%)
IC50=82 nmol/L
AGI-5198/(μmol/L)

1

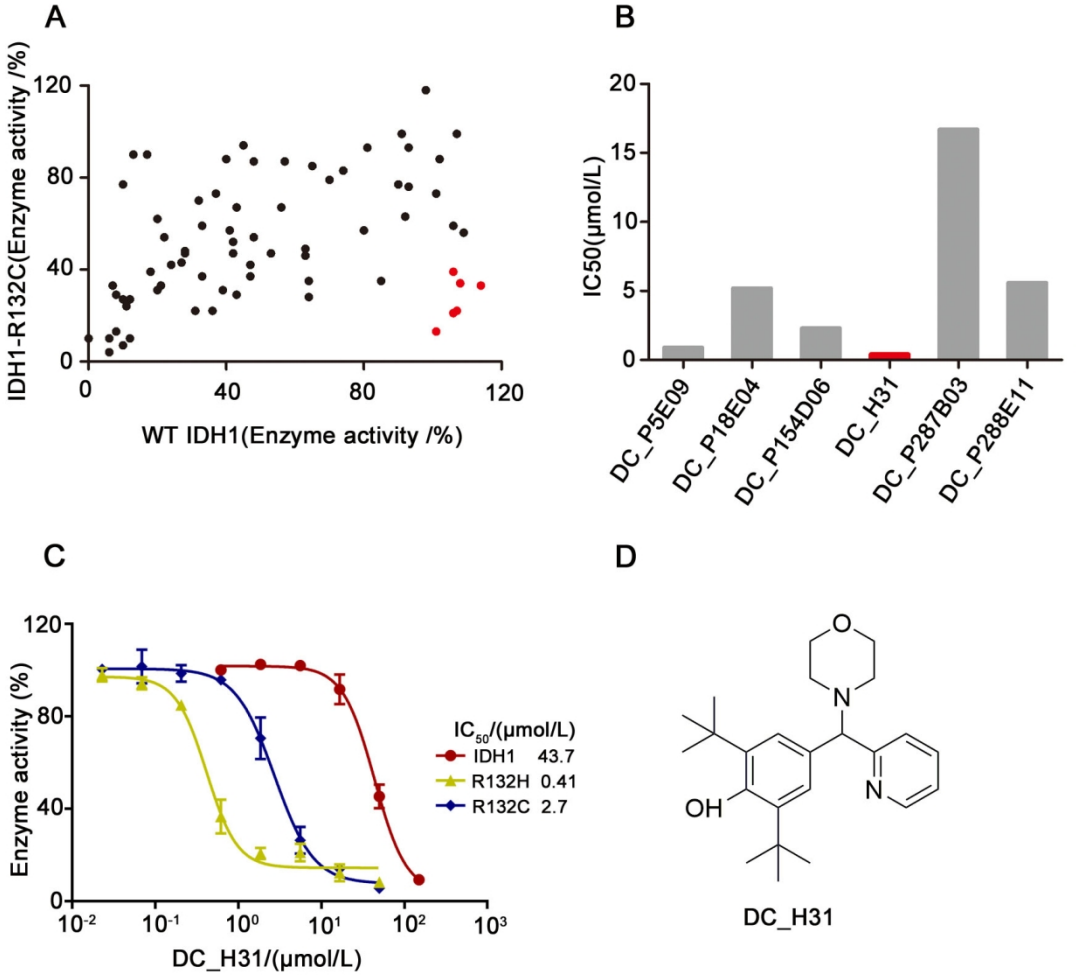
A
IDH1-R132C(Enzyme activity /%)
WT IDH1(Enzyme activity /%)
B
IC50(μmol/L)
DC_P5E09
DC_P18E04
DC_P154D06
DC_H31
DC_P287B03
DC_P288E11
C
Enzyme activity (%)
IC50/(μmol/L)
IDH1 43.7
R132H 0.41
R132C 2.7
DC_H31/(μmol/L)
D
DC_H31

2

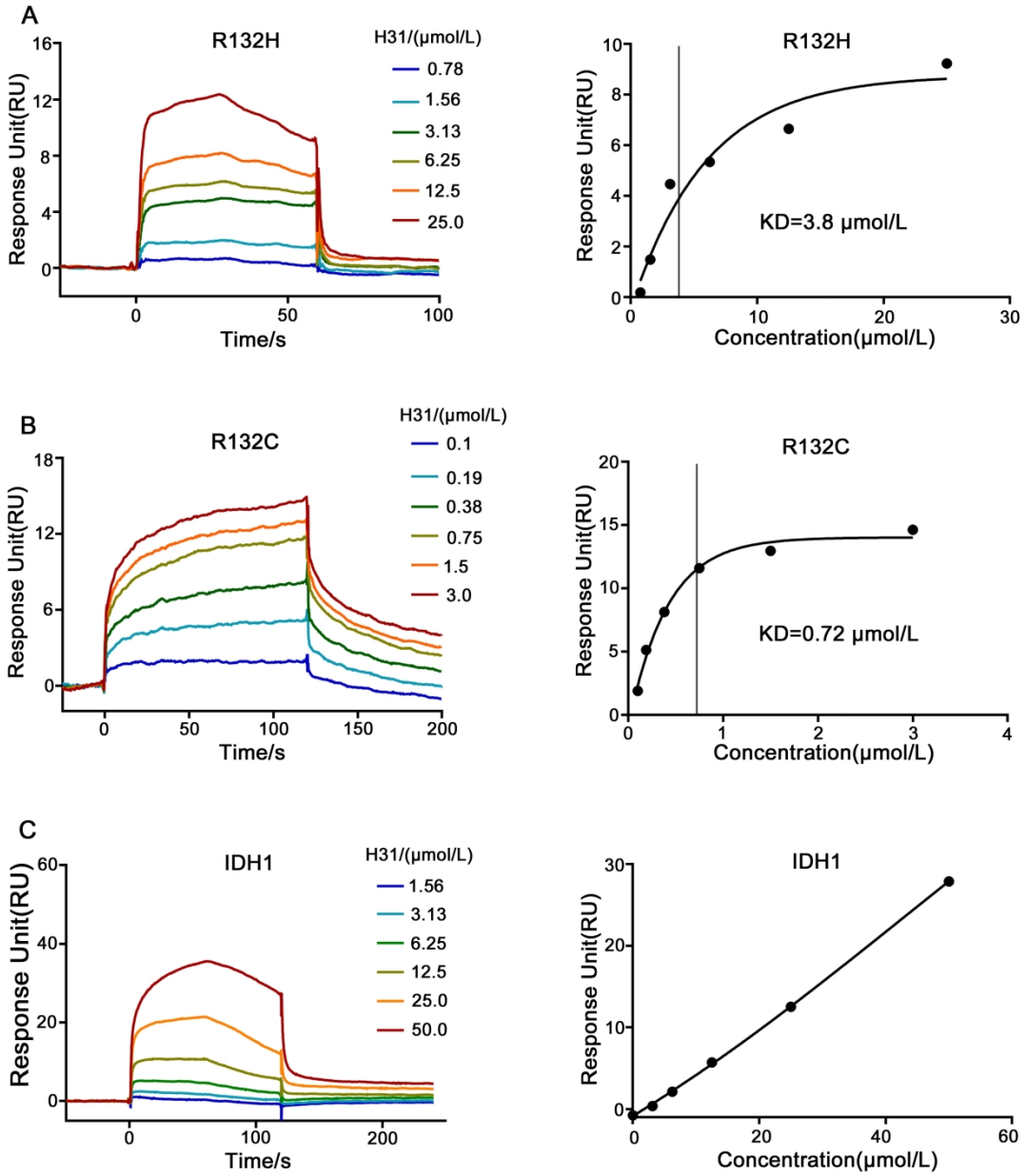
A
R132H
H31/(μmol/L)
0.78
1.56
3.13
6.25
12.5
25.0
Response Unit(RU)
Time/s
R132H
KD=3.8 μmol/L
Response Unit(RU)
Concentration(μmol/L)
B
R132C
H31/(μmol/L)
0.1
0.19
0.38
0.75
1.5
3.0
Response Unit(RU)
Time/s
R132C
KD=0.72 μmol/L
Response Unit(RU)
Concentration(μmol/L)
C
IDH1
H31/(μmol/L)
1.56
3.13
6.25
12.5
25.0
50.0
Response Unit(RU)
Time/s
IDH1
Response Unit(RU)
Concentration(μmol/L)

1

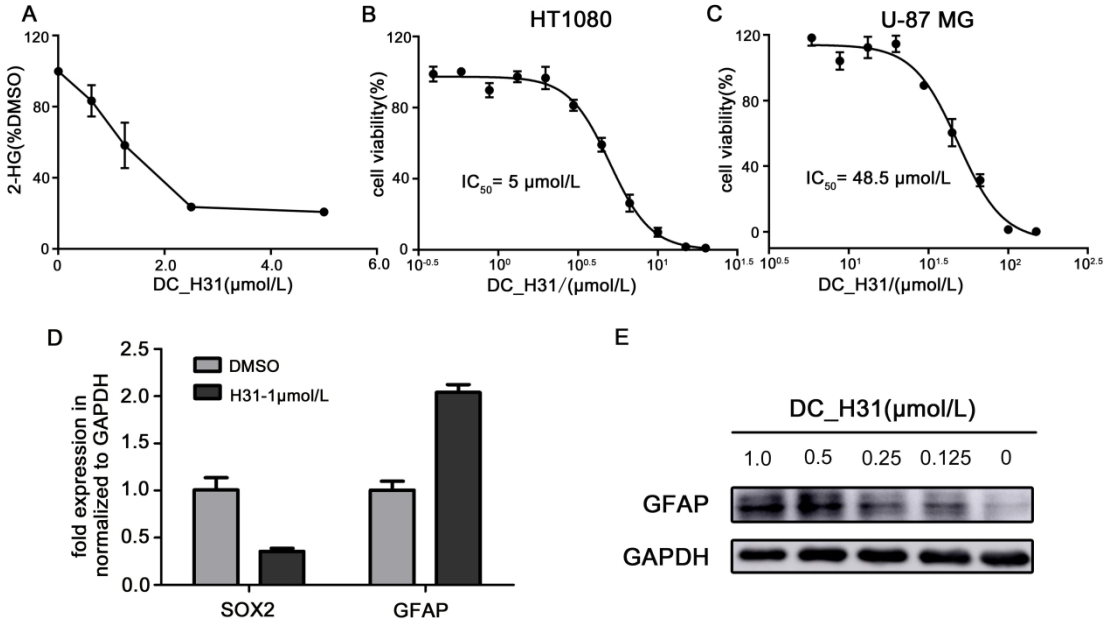
A
2-HG(%DMSO)
DC_H31(μmol/L)
B
HT1080
cell viability(%)
IC50= 5 μmol/L
DC_H31/(μmol/L)
C
U-87 MG
cell viability(%)
IC50= 48.5 μmol/L
DC_H31/(μmol/L)
D
DMSO
H31-1μmol/L
fold expression in normalized to GAPDH
SOX2
GFAP
E
DC_H31(μmol/L)
1.0 0.5 0.25 0.125 0
GFAP
GAPDH

1

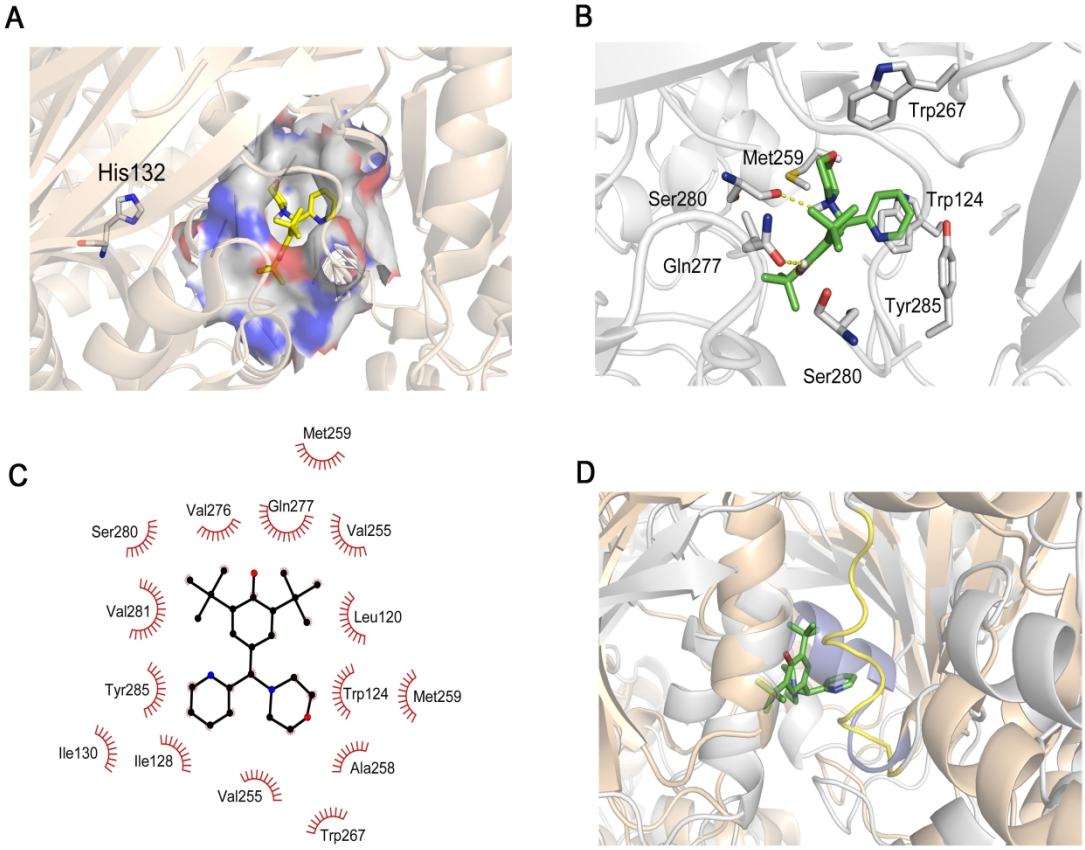
A
His132
B
Trp267
Met259
Ser280
Trp124
Gln277
Tyr285
Ser280
C
Met259
Val276
Gln277
Ser280
Val255
Val281
Leu120
Tyr285
Trp124
Met259
Ile130
Ile128
Ala258
Val255
Trp267
D

2